CrossMark

The sources and distribution of carbon (DOC, POC, DIC) in a mangrove dominated estuary (French Guiana, South America)

R. Ray · E. Michaud · R. C. Aller · V. Vantrepotte · G. Gleixner ·
R. Walcker · J. Devesa · M. Le Goff · S. Morvan · G. Thouzeau

Abstract Mangrove forests are highly productive coastal ecosystems that significantly influence global carbon cycling. This study characterized the sources of dissolved organic carbon (DOC), particulate organic carbon (POC) and dissolved inorganic carbon (DIC) and the processes affecting their distributions in a mangrove-influenced estuary located in French Guiana (FG), a region representative of these dynamic systems down drift of the Amazon River. Four sampling cruises were carried out between 2013 and 2015 in surface waters of the estuary during dry and wet seasons. Stable isotopes (δ^{13}DOC, δ^{13}POC, δ^{13}DIC), elemental ratios and optical properties (absorption) were used as proxies to identify different C sources. Property–salinity relationships revealed regions of approximately linear mixing (e.g., alkalinity) or net sources or sinks (e.g., DOC). DIC speciation and isotopic distributions demonstrated dynamic source–sink reaction processes within the estuary. DOC was the major form of organic carbon representing mixtures of terrestrial sources (e.g., pore water, litter leaching) and very high concentration (400–800 μM) compared to other mangrove settings (e.g. Brazilian, Sundarbans, African). Highly negative δ^{13}POC ($-40‰$) in the riverine part presumably suggests the role of freshwater phytoplankton in the

R. Ray (✉) · E. Michaud · J. Devesa ·
M. Le Goff · G. Thouzeau
Laboratoire des Sciences de l'Environnement Marin
(LEMAR), UMR 6539, (UBO/CNRS/IRD/Ifremer),
Institut Universitaire Européen de la Mer, rue Dumont
d'Urville, 29280 Plouzané, France
e-mail: raghab.ray@univ-brest.fr;
raghab.ray@gmail.com

R. C. Aller
School of Marine and Atmospheric Science, Stony Brook
University, Stony Brook, NY 11794, USA

V. Vantrepotte
Laboratoire d'Océanologie et de Géosciences (LOG),
Université du Littoral Côte d'Opale, 32 avenue Foch, BP
80, 62930 Wimereux, France

V. Vantrepotte · S. Morvan
USR LEEISA (Laboratoire Ecologie Evolution et
Interactions des Systèmes Amazoniens), 275 route de
Montabo, 97334 Cayenne, French Guiana

G. Gleixner
Department of Biogeochemical Processes, Max Planck
Institute for Biogeochemistry, Hans, Knoell Str. 10,
07745 Jena, Germany

R. Walcker
EcoLab, Université de Toulouse, CNRS, Toulouse,
France

dry season and methanotrophic sources derived from senescent mangrove deposits or upstream hydrothermal dam during the wet season. Microphytobenthos and marine phytoplankton were the primary sources of POC inshore and DOC offshore, respectively. Mangrove products and benthic microalgae dominated estuarine sources of C in FG coastal waters ($\sim$ 10 km, inner shelf region), and there was extensive exchange of C between forest and tidal flat and the estuarine reservoirs.

Introduction

Mangrove forests are confined to the tropical and subtropical regions, and are among the most productive coastal habitats with worldwide primary production of 218 ± 72 Tg C yr^{-1} (Bouillon et al. 2008; Fuentes and Barr 2015). Above-ground and below-ground carbon stocks in mangroves (956 Mg C ha^{-1}) are elevated compared to salt marshes (593 Mg C ha^{-1}), seagrasses (142 Mg C ha^{-1}) and rain forests (241 Mg C ha^{-1}) (Twilley et al. 1992; Donato et al. 2011; Alongi 2014) highlighting their potential role as 'blue carbon' stock (McLeod et al. 2011; Hutchison et al. 2014). Despite such a potential storage capacity, a significant part of mangrove-derived carbon is lost through tidal export of dissolved and particulate organic carbon (DOC and POC, respectively) and through respiration due to organic matter remineralization as CO_2 or CH_4. Those components finally enter into the ocean and atmosphere via rivers and estuaries (Maher et al. 2013, 2015). Therefore, such mangrove-influenced estuaries represent biogeochemically active zones where exchange of organic matter (OM) between forests, sediments, estuaries and the adjacent ocean takes place. These estuaries tend to be net heterotrophic globally and act as sources of CO_2 to the atmosphere (i.e. carbon mineralization exceeds carbon fixation, Borges et al. 2003; Abril et al. 2014; Ho et al. 2014). Labile OM provided by high mangrove productivity fuels heterotrophy, thus influencing dissolved inorganic carbon (DIC) composition (Gattuso et al. 1998). In addition to mangroves, other multiple C

sources (riverine, phytoplankton, benthic microalgae) and physical transport can play key roles in the processing of organic matter, sequestration, or mineralization within the coastal zone. These C sources and the relative importance of processes such as mixing or biogeochemical reactions can change over various time and spatial scales along the estuarine salinity gradient. In fact, the relationships of C components, such as DOC, POC, and DIC to salinity, a conservative tracer, can be utilized to infer the dominant inputs or losses and the mixing of C in the different coastal water masses (e.g., Loder and Reichard 1981; Bauer and Bianchi 2011; Canuel and Hardison 2016).

In these dynamic coastal systems, elemental ratios (C: N) and stable isotopes ($\delta^{13}C$, $\delta^{15}N$) can be applied as proxies to identify the mixture of organic matter sources (Kuramato and Minagawa 2001; Raymond and Bauer, 2001; Kennedy et al. 2004; Ralison et al. 2008; Ray et al. 2015). In general, terrestrial OM has lower $\delta^{13}C$ values than marine OM (Lamb et al. 2006). Furthermore, these proxies can be used to explain the fate of estuarine OM based on the isotopic fractionations caused by physical, chemical, and biological processes. For example, OM degradation driven by microbial activities results in the enrichment of isotopic values due to the preferential decomposition of $^{13}C/^{15}N$ depleted compounds (Lehmann et al. 2002).

Dissolved organic compounds can be discriminated both isotopically and optically. Application of these tools has advanced our understanding of carbon cycling in global mangrove ecosystems (Dittmar et al. 2001; Bouillon et al. 2007a, b; de Rezende et al. 2007; Maher et al. 2013; Ray et al. 2015; Leopold et al. 2016). Optical properties of colored dissolved organic matter (CDOM) allow qualitative and quantitative assessment of DOC composition and sources (Vantrepotte et al. 2015). Optical descriptors such as the absorption coefficient (a_{cdom}), spectral slope (S) and absorption normalized to DOC provide further insights into various characteristics of DOM (Helms et al. 2008; Fichot and Benner 2011). Recent advances in measuring in stable isotopic composition of DOC potentially allows a more complete resolution of the sources, transport, and transformation of DOM in the mangrove aquatic systems (Ralison et al. 2008; Ray et al. 2015). However, simultaneous measurements of stable isotopic composition in both organic and inorganic carbon are still very few. Identifying the

origin and fate of the different carbon species is particularly important for the very dynamic mangrove systems like in French Guiana (FG hereafter).

The FG coast is characterized by migrating offshore mobile mudbanks derived from the huge sediment input from the Amazon River (Anthony et al. 2010). These inputs are characterized by very high OC remineralization rates (Aller and Blair 2006) and low sedimentary organic carbon (OC) content ($\sim 0.7\%$). The intertidal mud banks, when stabilizing, are then rapidly covered by benthic microalgae (microphytobenthos as Diatoms, Cyanophycae) (Sylvestre et al. 2004; Debennay et al. 2007; Gensac et al. 2015) and colonized by mangroves stands of different ages that increase sedimentary organic carbon content (Marchand et al. 2003, 2004). Sedimentary OC thus depends directly on the mangrove stand structure such as stand age, species composition, tree height, diameter and density (Fromard et al. 2004). The OC increase is not as high as those in terrestrial forests probably due to tidal export of mangrove-derived OM to the ocean which would balance low mineralization rates in mangrove sediments (Marchand 2017). Generally low sedimentary OC is somewhat of a paradox because FG mangroves occupy $\sim 80\%$ of the Guianese littoral, with high standing biomass (31–350 Mg C ha^{-1}, Fromard et al. 1998), high litter fall rates (4.0–5.8 Mg C ha^{-1} yr^{-1}, Betoulle et al. 2001) and extremely fast growth rate (150 cm yr^{-1}, Proisy et al. 2009), this latter property being a likely adaptation to the dynamic coastal system.

In French Guiana, much of the OC that forms the initial basis for sediment formation in the mangrove forest is either marine OC imported from the offshore mobile mud stream and colonized by mangroves (Aller and Blair 2006), entrained phytoplankton, or OC derived from the benthic microphytobenthos (Gontharet et al. 2014). Thus, there is an active exchange of OC both into and out of the FG mangroves. However, the contributions of different potential sources to the OC pool in adjacent waters are still unknown. Previous studies in the Sinnamary area were either conducted in the riverine part (Petit-Saut hydroelectric dam; Abril et al. 2005; Guérin et al. 2006) or offshore of the estuary (Vantrepotte et al. 2015). How the mixing of different water masses along the estuarine salinity gradient changes the sources and biogeochemistry of C species (i.e. DOC, POC, and DIC) has not been previously investigated.

Seasonal effects are likely as well, because FG mangrove environments are in a sub-equatorial climate, i.e. alternating between dry and rainy seasons. Previous studies in other tropical estuaries and mangroves have shown considerable seasonality in the concentrations and sources of OC (Chen et al. 2013; Cawley et al. 2013; Ray et al. 2016). Up to now, there has been no record of seasonal patterns for DOC, POC and DIC in the FG estuarine systems.

In this study, we examine the sources of DOC, POC, and DIC and the processes affecting their distributions in a mangrove-influenced estuary located in French Guiana. Given the high mangrove productivity, litterfall rates and sediment loading, it is hypothesized that the mangroves and mudbanks bordering the estuaries and coastal margin in French Guiana are the major contributors of estuarine organic and dissolved inorganic carbon. Therefore, this study aims: (1) to characterize spatio-temporal distributions and mixing of DOC, POC and DIC along the surface waters of a representative estuarine system in FG; (2) to identify their sources and fate on spatio-temporal basis; and (3) to understand the role of mangroves on overall biogeochemistry of the organic and inorganic carbon pools in the estuary.

Materials and methods

Study area

The study area is the estuarine mouth of the Sinnamary River (6 km^2) and the adjacent coastal zone, 50 km northwest of Kourou, French Guiana (South America) (5°26′–5°31′N and 52°59′–53°W) (Fig. 1). The Sinnamary River has seasonal and inter-annual variations of water discharge that depend on multiple factors such as the opening of the "Petit-Saut" dam during the wet season or El Nino Southern Oscillation (ENSO) events (Maia de Oliveira and Clavier 2000; de Merona 2005). The average Sinnamary river flow varied between 193 and 700 m^3 s^{-1} during study periods in 2015 with maximum and minimum discharge found in June (wet season) and November (dry season) respectively (source: DEAL GUYANE-EDF). The estuary is a macro-tidal, semidiurnal type with spring and neap high tide water levels up to 3.2 m and 2.5 m respectively. It has an average depth of 3–4 m and a watershed area of 6900 km^2 (Abril et al. 2005). The
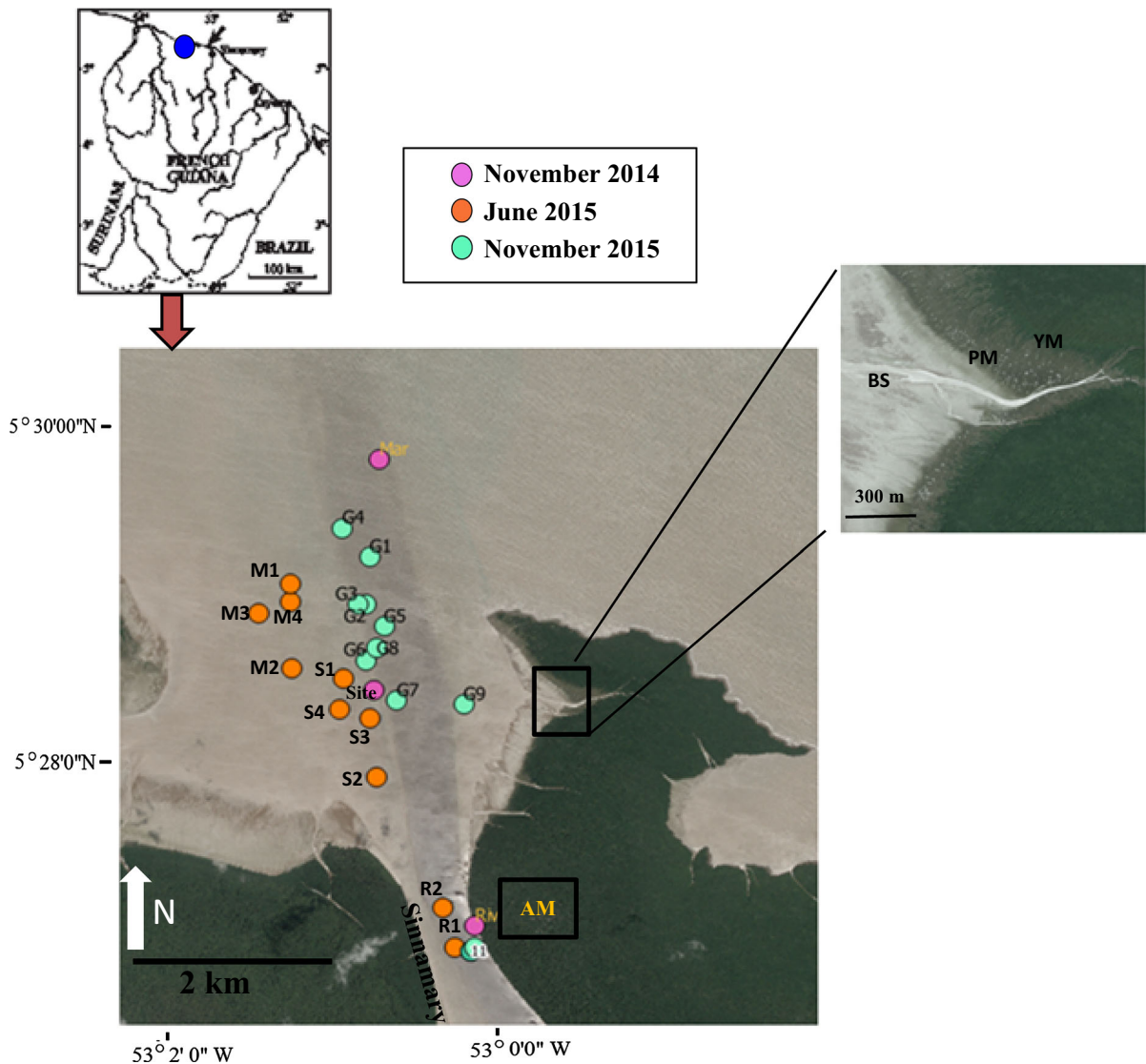
Fig. 1 Study area located north-west of the Sinnamary estuary in French Guiana. Locations of the four stages of mangrove development (BS: bare sediment, PM: pioneer mangroves, YM: young mangroves and AM: adult mangroves) in the outlined squares and insert. Surface water sampling sites are shown for 2014–2015. Latitude and longitude of the OW series largely resembled with those of the G series (according to geographical positioning system), hence, they are not shown for clarity of the map Image source: @CNES (2015) and Astrium Services/ PLEIADE lmages (09/17/2015), all rights reserved, out of commercial used. Image processing R. Ray (University of Western Brittany)

lower reach is bordered by thick mangrove forest. Perhaps the most unique feature of these mangroves is the occurrence of their growth stages across the intertidal mudflat according to their structural and biological features: pioneer, young, adult, mature, mixed and cemetery stands (Fromard et al. 2004). During mud bank stabilization, pioneer mangrove stands are established on newly exposed mud, and upon successive arrival of additional seeds, the mangroves are gradually structured into growth stages. These mangrove stages in French Guiana, including the Sinnamary area, have been previously studied in detail from ecological and structural points of view (Fromard et al. 1998; Fabre et al. 1998). The vegetation is composed predominantly of monospecific stands of *Avicennia germinans* (Linnaeus) Stearn, a

species adapted to rapid sedimentary changes. *A. germinans* is sometimes associated with *Laguncularia racemosa* (L.) Gaert, *Rhizophora* Spp. (*R. mangle* L. or *R. racemosa* Meyer) and *Pterocarpus officinalis* mangrove trees in areas situated far from coastal sedimentary processes. At the limit with freshwater environments, species characteristic of flooded forest, including *Symphonia globulifera*, *Virola surinamensis*, *Ficus* sp. and *Euterpe oleracea,* colonize the undergrowth of old *A. germinans* stands (Proisy et al. 2007).

The climate is sub-equatorial, driven by the annual migration of the inter-tropical convergence zone (ITCZ) that produces a long wet season (April to July), a long dry season (July to November), a short wet season (November to February) and a short dry season (February to April). Annual rainfalls reach 2500–3000 mm yr^{-1} (Marchand et al. 2003). Air temperature recorded in this study ranged from 25 to 30 °C in June and 27.1 to 30 °C in November of the year 2015.

Remote sensing application

Mapping of mangrove age in 2015

A map of mangrove age in the vicinity of the Sinnamary River during the year of field sampling was constructed by analysis of time series of aerial and satellite images dating back to 1950 (Table S1, supplementary). Overlaying of successive images acquired during this period enabled the dating of newly established mangrove areas and thus "theoretical" ages of mangrove trees in 2015 as previously shown in Fromard et al. (2004). Digital archives of aerial photographs (1950, 1955, 1976, 2005) were retrieved at the French National Institute of Geographic and Forest Information (IGN) and are available at https://remonterletemps.ign.fr/. A declassified ARGON satellite photograph from 1963 was also used and is available at https://lta.cr.usgs.gov/declass_1. For the most recent period, LANDSAT satellite images (1985, 1990, 1992, 1997, 2003, 2007, 2008, 2010, 2011, 2013, 2014) were obtained from https://glovis.usgs.gov/. The dataset was completed with SPOT (1995, 2000, 2001, 2002, 2004, 2006, 2009) and PALEIADES (2012, 2015) satellite images obtained from http://www.astrium-geo.com/geostore/. Using the ARCGIS software package (ESRI, Redlands, CA,

USA), images were geo-rectified based on the orthorectified map BD Ortho 2005 as the target raster dataset for identifying ground control points and aligning images (Walcker et al. 2015). Maps of mangrove cover over the study area were manually digitized by photointerpretation on the computer screen and overlaid in order to derive a map of mangrove ages in 2015. The map of mangrove ages determined from the changes in mangrove extent since 1950 is a raster file image shown in Fig. 2.

Field sampling

Four field campaigns were conducted in the Sinnamary estuary at different seasons between 2013 and 2015 (dry and wet seasons). Water sampling was performed along the salinity gradient covering riverine, estuarine and marine zones. Sampling stations were located near the mouth of the Sinnamary River and extended offshore 0.3–4 km from the mangrove fringe (Fig. 1). Satellite maps in high spatial resolution (PLEIADES satellite imaging, 50 cm) provided accurate sampling site locations at each sampling time. Sampling was mostly conducted during the spring tides except the two cruises in 2014. In October 2013, surface waters were collected at high tide from seven stations along the estuary (OW1-7), while in October 2014, they were collected from a total of 13 stations (Mar, Site, Riv and OW1-10) covering both high and low tide. In 2015, 10 stations were sampled (M1-4, S1-4 and R1-2) at high tide in June and 11 stations (G1-11) at high tide in November. Coordinates of the sampling stations in 2013–2014 (i.e. OW series) largely correspond with locations of the G series, hence, OW points are not shown for clarity.

Water samples were manually collected with acid cleaned Nalgene bottles (1L) from ∼ 0.3 m below the surface at each station for field measurement of physico-chemical parameters (temperature, salinity and pH) and filtration and storage of samples for biogeochemical analyses. Total alkalinity (TA), Dissolved Inorganic Carbon (DIC), Dissolved Organic Carbon (DOC), their isotopes (δ^{13}DIC, δ^{13}DOC), Colored Dissolved Organic Matter (CDOM) and particulate parameters (total suspended matter (TSM), Particulate Organic Carbon and Nitrogen (POC and PN, respectively) in the TSM pool, δ^{13}POC, δ^{15}PN and photosynthetic pigments) were sampled during these cruises (Table 1).

Fig. 2 Satellite image originating age mapping of the mangroves located at the north-west of the Sinnamary estuary in French Guiana. Areas with mangroves < 1 year-old immediately adjacent to 1 year-old mangrove regions are left in dark gray Source: @CNES (2015) and Astrium Services/PLEIADE IMAGE (09/17/2015). all rights reserved, out of commercial use. Image processing R. Walcker (University of Paul Sabatier, Toulouse)
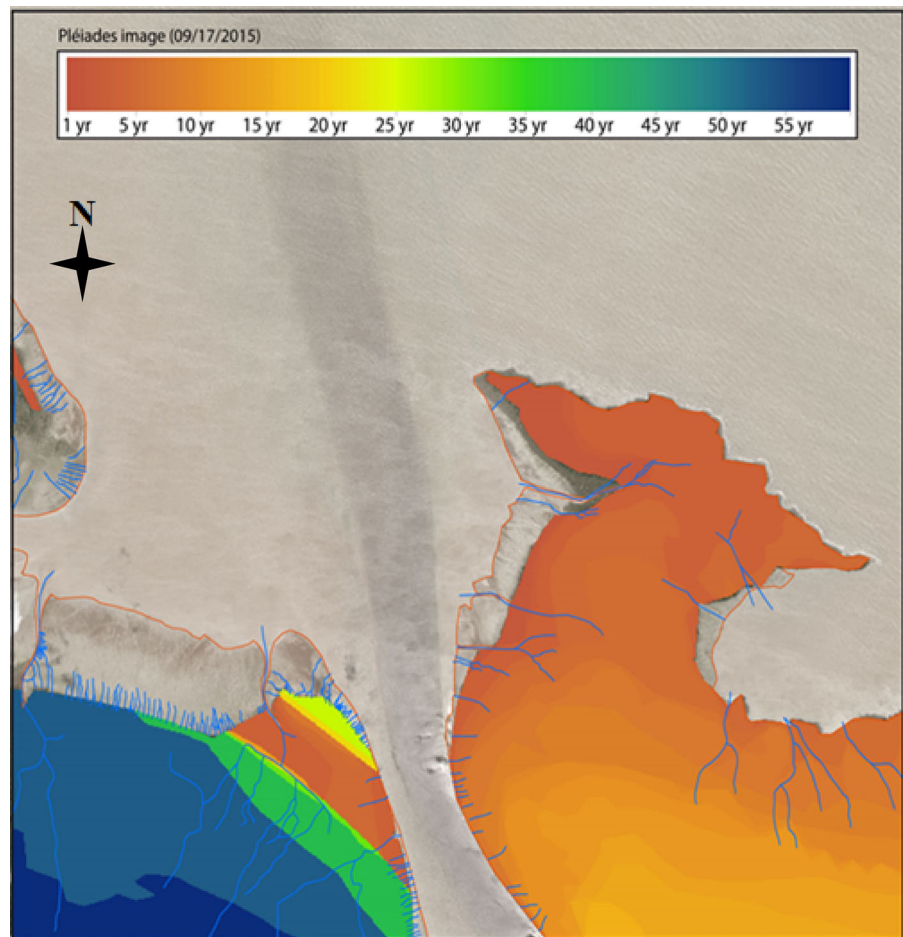
Carbon, nitrogen and their isotopes were also measured in the potential sources, i.e. surface sediment, fresh *Avicennia* leaves, litter and microphytobenthos (MPB), which were collected in bare sediment, pioneer, young and adult mangrove sites. Only surface sediment was sampled in duplicate at each site. These samplings were carried out in both seasons of 2015 at low tide (refers to Table 1). MPB was collected by gently scraping off the visible mats from the sediment surface (following Gontharet et al. 2014). MPB is referred here as 'mixed MPB' due to contamination with the bulk sedimentary OC (discussed in Sect. Sources of sedimentary TOC, TN). The top 2 cm surface sediment was collected by using a push-up PVC corer (10.3 cm inner diameter) and subsampled (2.7 cm i.d) in the laboratory for weighing and analysis. Pore water DOC samples were collected from each mangrove sites by extracting sediment obtained with same corers. Rhizon samplers consisting of small microporous polymer tube (2.5 mm diameter, pore size of the membrane < 0.2 μm) connected to a syringe (50 ml capacity) through a standard luer-lock connector were used to extract pore water from the upper 2 cm of the core (Buckingham et al. 2008) (typical retrieval of 8–10 ml, retrieval time of ∼ 10–30 min for DOC).

Analytical procedure

Physico-chemical parameters

Temperature, salinity and pH were measured directly in the field using a multiparameter water quality meter (WTW Multi 3500i) with a precision of ± 0.1 salinity, ± 0.1 °C temperature, and pH, the latter calibrated with NBS buffers (precision of 0.01%). Additionally, YSI 6920v2 probes (YSI Inc., Yellow Springs, OH, USA) were deployed (∼ 0.3 m below

Table 1 Details about the sampling periods, tides, stations name and measured parameters during the 2013–2015 cruises in and nearshore the Sinnamary estuary

Year	Season	Date	Lunar period	High tide	Low tide	Sampled period	Stations	Measured parameters
2013	Dry	Oct 26	End of spring tides	6:00/ 18:00	~ 2:10	HT − 2 h	OW1 to OW7	pH, TA
2014	Dry	Oct. 20	Neap tides	15:25	9:16	HT + 1 h	OW1 to OW10	pH, TA, DIC
2014	Dry	Oct. 30	Neap tides	9:26	15:34	HT to LT	MAR, SITE, RIV	pH, TSM, TA, DIC, POC, PN, pigment
2015	Wet	June 8	End of spring tides	8.59	15:21	HT + 3 h	M1 to M4, S1 to S4, R1 and R2	pH, TSM, TA, DIC, POC, PN, DOC (tidal + porewater), CDOM, δ^{13}DIC, δ^{13}POC, δ^{13}DOC, δ^{15}PN, pigment
2015	Dry	Nov 17	End of spring tides	8:20	14:32	HT + 4 h	G1 to G11	pH, DO, TSM, TA, DIC, POC, PN, DOC (tidal + porewater), CDOM, δ^{13}DIC, δ^{13}POC, δ^{13}DOC, δ^{15}PN, pigment
End members collection (sediment, leaf, litter, MPB)								
2015	Wet	June 3 to 5	Mid of spring tides	5:06 to 6:27	11:21 to 12.45	LT + 1 h	BS, PM, YM	TOC, TN, δ^{13}C, δ^{15}N
2015	Wet	June 8	End of spring tides	8.59	15:21	LT-3 h	AM	TOC, TN, δ^{13}C, δ^{15}N
2015	Dry	Nov 12 to 15	Mid of Spring tides	5:07 to 6:48	11:27 to 12:53	LT + 1 h	BS, PM, YM, AM	TOC, TN, δ^{13}C, δ^{15}N

the water surface) to measure dissolved oxygen (DO) at each station (G1 to G11) in the dry season of 2015, whereas only two data sets from surface water (station S4 and R2) were retrieved during the wet season. Chloride concentrations (Cl) measured by potentiometry were used to calculate salinity of the water samples (S = 1.806 Cl; Strickland and Parsons, 1968) in the wet season of 2015.

Biogeochemical parameters

Dissolved: DOC, δ^{13}DOC, CDOM, DIC, δ^{13}DIC Water samples were filtered under gentle vacuum for dissolved parameters (DOC, δ^{13}DOC, CDOM, DIC and δ^{13}DIC). Filtrates were distributed in 25 ml screw-capped glass vials for TA and δ^{13}DIC measurements, and overfilled without any bubble formation. For DOC and δ^{13}DOC analyses, water samples were filtered through precombusted GF/F filters (0.45 μm), acidified with 0.2 M HCl until pH 2, and stored in 60 ml precombusted amber glass bottles under refrigeration (4 °C). Pore waters in Rhizon syringe tubes were also preserved the same way to prevent

bacterial degradation. CDOM samples were filtered under gentle vacuum (< 5 mm Hg) through 0.2 μm polycarbonate membranes (Whatman Nuclepore, 47 mm) and stored frozen in brown glass bottles.

DOC concentrations (μM) were measured by High Temperature Combustion Oxidation (HTCO, Shimadzu TOC-VCSH) (Ray et al. 2105). 100 μL injections of every sample were repeated (three to five times) until the coefficient of variation of the measurements decreased below 2%. The accuracy of DOC measurements was checked at device startup and then every six samples using the deep-sea water consensus reference material (CRM, Hansell Laboratory, Rosenstiel School of Marine and Atmospheric Science, University of Miami) from batch 12, 2012 (41–44 μmol L^{-1}). Calibration curves were computed using potassium hydrogen phthalate solution (KHP) ranging from 10 to 400 μM. Measurements of DOC δ^{13}C (δ^{13}DOC) were carried out by wet chemical oxidation (WCO) using a HPLC system coupled to a Delta$^+$ XP IRMS through a LC IsoLink interface (Thermo Fisher Scientific, Germany). This is a flow injection method (for instrumental details refer to

Scheibe et al. 2012). Advantages of measuring δ^{13}DOC by LC-IRMS over EA-IRMS are that very small sample volume is required (25 µL), processing is faster and there is no need of derivatization; unlike EA-IRMS that normally causes isotopic fractionation (Hettmann et al. 2007). However, halides can react during WCO and cause interferences in the LC-IRMS method. To circumvent potential interference (here as Cl$^-$), concentrated potassium per sulphate (Na$_2$S$_2$O$_8$ of $\sim$ 2 M) was added to the oxidation chamber as prescribed by Osburn and St-Jean (2007). Following Scheibe et al. (2012), halide interference was however assumed to be very low because of high DOC concentrations in the estuarine samples, averaging 500 µmol L^{-1}, substantially higher than normal oceanic water (80–100 µmol L^{-1}). Linearity of the system was tested by varying concentrations (5–40 mgC L^{-1}) of citric acid (δ^{13}C: $-$ 18.58 ‰$_{VPDB}$; Fluka, Germany) and pulses of CO$_2$ reference gas (δ^{13}C: $-$ 38.16‰$_{VPDB}$) were used for calibration of the LC-IRMS system during every chromatographic run that lasted for 20 min. The δ^{13}DOC values are reported relative to the PDB standard with an overall uncertainty of $\pm$ 0.10‰. CDOM absorption spectra were measured following the NASA protocol (Mitchell et al. 2003) every nanometer from 250 to 850 nm using a double-beam Ultraviolet–Visible spectrophotometer (Shimadzu, UV-2450).

Analysis of total alkalinity (TA) was performed in the laboratory by means of gran titration (Automatic Potentiometric Titrator) with 0.1 N HCl with accuracy better than 10 µM. Alkalinity was also measured using a 96 well plate method adapted from Sarazin et al. (1999) and optimized for the analytical range 0–3 meq L^{-1}. DIC and pCO$_2$ were calculated using CO$_2$SYS (Lewis and Wallace 1998), with the carbonate dissociation constants K1 and K2 from Hansson, (1973) refitted by Dickson and Millero (1987), and pH measured on the NBS scale. For the analysis of the δ^{13}DIC, a 2 mL headspace was created which was filled with helium and 300 µL of H$_3$PO$_4$ were added to convert all inorganic carbon species to CO$_2$. After overnight equilibration, part of the headspace was injected into the helium stream of an EA-IRMS (Thermo Finnigan Flash HT and Thermo Finnigan DeltaV Advantage) for δ^{13}C measurement of water (Gillikin and Bouillon 2007).

Particulate: TSM, POC, PN with their isotopes (^{13}C, ^{15}N) and pigments Filtered water samples residues were used for separate measurements of particulate parameters (TSM, POC, PN, δ^{13}POC, δ^{15}PN and photosynthetic pigments). For chlorophyll-a (Chl-a) and pheopigment (Pheo) analyses, 150 ml of water was filtered through 47 mm Whatman GF/F filters which were kept frozen thereafter. Pigments (Chl-a and Pheo) were extracted for approximately 12 h in 10 mL of 90% acetone at 4 °C and analyzed with a Turner AU-10 Fluorometer. Chl-a extracts were acidified with 1 N HCl for pheophytin measurements. Pheo:Chl-a ratios were calculated to assess phytodetritus degradation state. Samples for TSM were stored in a cooler after filtration of 200 ml tidal water on preweighed and precombusted (overnight at 450 °C) 47 mm Whatman GF/F filters (0.45 µm mesh size), and subsequently oven dried at 50 °C for 24 h and weighed. Elemental and isotopic samples of POC and PN were collected using 25 mm Whatman GF/F (0.45 µm mesh size) filters and subsequently freeze dried.

For POC and PN analyses, the weighed GF/F filters were transferred into 10 × 10 mm tin cups, encapsulated and placed into an autosampler. For organic carbon analysis, samples were treated with HCl fumes for 4 h to remove inorganic C (CaCO$_3$) and kept in oven at 40 °C for 2 h after which they were transferred into silver cups of 10 × 10 mm, and dried at 40 °C for 24 h prior to measurements. The encapsulated samples were then analyzed by combustion at 930 °C on a CHN carbon analyzer (FLASH-2000). Relative uncertainty in the measurement of C and N were $\pm$ 0.1 and $\pm$ 0.03%, respectively.

A ThermoFinnigan Delta plus mass spectrometer coupled with a EA Flash 2000 and ConFlo IV inter face was used for analyzing δ^{13}C and δ^{15}N of the suspended matter. Sample preparation for the analyses was the same as for OC and ON; except that, 5 × 12 mm silver and tin capsules were used for sample collection and processing. All isotopic data are expressed in δnotation, such that δ value (‰) = [(R$_{sample}$/R$_{standard}$) $-$ 1] × 1000; where the isotopic ratios (R) of ^{13}C/^{12}C are expressed relative to the international PDB standard and ^{15}N/^{14}N relative to Air. Relative uncertainties in the measurement of δ^{13}C and δ^{15}N were $\pm$ 0.2 and 0.04‰, respectively.

The same procedure was followed for the determination of total organic carbon (TOC) and total nitrogen

(TN) and their isotopes (δ^{13}C, δ^{15}N) of the powdered sediment, MPB, leaf and litter samples.

Mixing models (conservative and non-conservative)

In order to quantify the addition or removal of DOC/POC/DIC by biogeochemical processes along the salinity gradient in the Sinnamary estuarine zone, a simple two component mixing model was applied (modified from Carpenter et al. 1975; Officer 1976),

$$C_{mix} = fC_R + (1 - f)C_M \qquad (1)$$

where f represents the salinity (S) fraction (f = 1 − S/35) and C_R and C_M are the fixed riverine and marine endmember concentrations, respectively; C_{mix} denotes C derived by conservative mixing. Positive/negative differences of an observed concentration, C_{obs}, from C_{mix} in Eq. 1 indicate sources/sinks or the transformation of C in the estuary.

Residual C concentration or ΔC, at any given salinity within the salinity gradient can be estimated:

$$\Delta C = (C_{obs} - C_{mix}) \qquad (2)$$

Stable isotope compositions are included in this mass–balance equation to constrain the sources/sinks of C following the general conservative mixing equation (adapted from Mook and Tan 1991):

$$\delta^{13}C_{mix} = \frac{(C_R\delta^{13}C_R - C_M\delta^{13}C_M)S + (S_R C_M\delta^{13}C_M - S_M C_R\delta^{13}C_R)}{(C_R - C_M)S + (S_R C_M - S_M C_R)} \qquad (3)$$

where $\delta^{13}C_{mix}$ is the predicted conservative isotopic composition, $\delta^{13}C_R$ and $\delta^{13}C_M$ are the riverine and marine endmember isotopic compositions, respectively, and S_R and S_M are the salinities of the two endmembers. All endmember compositions are assumed constant.

The isotopic composition of the residual component, $\delta^{13}C_{\Delta C,}$ can be estimated as:

$$\delta^{13}C_{\Delta C} = \left(\delta^{13}C_{obs}C_{obs} - \delta^{13}C_{mix}C_{mix}\right)/(C_{obs} - C_{mix}) \qquad (4)$$

The concentration and isotopic composition balance calculations (Eqs. 1–4) were applied to DOC/POC/DIC. Due to the paucity of marine endmember data in the wet season, estimates of the different components were calculated only for the dry season.

Results

Map of mangrove stages

Mangrove stages in 2015 in the studied area were mapped using stand age as the main proxy (Fig. 2). The studied area was defined as a square area of 3527 ha situated at the mouth of the estuary where the sampling points were located. Mangroves in 2015 covered 1134 ha and bare mud was 244 ha at tide level 1.65 m above the lowest astronomical tide (Chat datum). The mature stands from about 30 to 60 years-old were found on the left side of the river, in the south-west hand corner of the studied area and accounted for 332.4 ha (Table 2). On the right side of the Sinnamary River, mangrove stands were from 1 to 15 years old. Pioneer, young-pioneer, young and adult stands accounted for 36.4, 347.6, 348.7, and 69 ha; respectively.

Physicochemical parameters

The Sinnamary surface water was characterized by a pronounced salinity gradient (varying from 0 near the mouth to 35 offshore). Maximum salinity range was recorded during the dry season in 2015 (0–35, G series) and minimum in the wet season (0–25, M-S-R series). Water temperature variations along the salinity gradient were relatively small for both the dry (29.2–31.2 °C) and wet (26.4–27.2 °C) seasons. Overall water temperature was 3 °C higher in the dry season than in the wet season in 2015. Dissolved oxygen (DO) varied between 150 μM and 186 μM (M = moles L^{-1}) along the estuary in the dry season in 2015. In general, DO concentration and saturation (%) were lower in the riverine sites (165 ± 1.3 μM, and 67 ± 1.4% respectively; stations R2 and G11, at S = 0) compared to the marine endmember and transitional sites (174 ± 8.8 μM and 82.5 ± 3.9%; S = 10–35). A summary of the other physicochemical parameters is given in Table S2 (supplementary).

Biogeochemical parameters

Dissolved and particulate organic carbon

DOC concentrations ranged between 808 and 109 μM (n = 42) between 0 and 25 salinity range in 2015 (dry season: 723 ± 62 μM stations G2, G5 to G11; wet

Table 2 Age and surface area of different mangrove facies from pioneer to mature mangroves in the study area

Mangrove stage	Stand age (yr)	Surface (ha)
Pioneer	1	36.44
Young-Pioneer	2	8.44
	3	141.17
	4	85.54
Young	5	90.26
	6	22.17
	7	84.46
	8	63.20
	9	19.28
	10	22.64
Adult	11	46.52
	12	66.59
	13	46.03
	14	46.31
	15	7.95
	15–19	0.43
	19–21	3.32
	21–26	6.56
Mature or mixed	26–31	4.36
	31–40	51.20
	40–53	221.96
	53–61	59.19

season: 485 ± 79 μM, stations M-S-R). The river endmember value was lower during the wet than the dry season. The δ^{13}DOC widely varied along the estuary (n = 21), ranging between -23.1‰ and -29.5‰ (minimum at G11, S = 0 and maximum at G1, S = 35) in dry season, whereas in the wet season it remained lower at all stations (-29.8 ± 1.3‰; no marine endmember was measured). DOC showed a non-conservative decreasing trend along the salinity gradient in the wet season whereas in the dry season, the distribution was more stable up to salinity 30 after which there was a sharp decrease of concentration to the marine endmember (Fig. 3a). The δ^{13}DOC exhibited enrichment of ^{13}C with increasing salinity in the dry season (Fig. 3b). Similar to the DOC distribution pattern, the CDOM absorption coefficient at 412 nm, $a_{cdom}(412)$ was highest at the riverine sites (4.25 m^{-1} at G11; 5.25 m^{-1} at R2) and lowest at the marine end (0.56 m^{-1} at G4) (Fig. 3c). Lowering of absorption values was more pronounced for the dry season up to

salinity 10–15. Like DOC and δ^{13}DOC, CDOM also behaved non-conservatively in both seasons. Slope at 275–295 nm ($S_{275-295}$) showed an increasing trend along the salinity gradient with higher values in the dry season than in the wet season (ranging 0.013–0.018 nm^{-1} and 0.012–0.014 nm^{-1}, respectively; n = 20, Fig. 3d). The ratio between colored DOM and carbon content of the DOM pool was described as $a_{cdom}(412)$/DOC (hereafter $a_{cdom}^*(412)$) and mirrored the changes of CDOM along the estuary (Fig. 3e). In the pore water, DOC concentrations varied between 964 and 1709 μM with the highest and lowest DOC values recorded for pioneer and adult mangroves, respectively (Table 3).

There was an overall slight increasing trend for total suspended matter (TSM) with increasing salinity (6.8–57 mg L^{-1} for S = 0; 178 mg L^{-1} for S = 35). TSM did not change much in concentration between the three sampling periods in 2014–2015, except two high values at higher salinities in October 2014 (Fig. 4a). The distribution pattern of POC was generally stable along the salinity gradient ranging from 16.6 to 101 μM (n = 34), except two points showing abrupt increase (up to 298.4 μM) corresponding to elevated TSM values within the salinity range 30–32 during October 2014 (Fig. 4b). The contribution of POC to total TSM pool did not vary much with season and was typically low in the salinity range 5–35 (generally between 0.2 and 1.7%) but somewhat higher at the riverine sites (up to 10.5%) (Fig. 4c). Except for the marine endmember in the 2015 dry season (-30.4‰), the δ^{13}POC varied from -41.8‰ to -36.3‰ (n = 19), and did not change much with season (Fig. 4d). The PN distributions followed similar patterns to POC and ranged between 1.2 μM and 14.9 μM (n = 34) except for the two points corresponding to high TSM values in October 2014 (up to 40.6 μM, Fig. 4e), whereas δ^{15}PN ranged between -1.4‰ and 3.3‰ (data not shown). Elemental atomic ratios (POC/PN) of suspended matter varied from 2.8 to 28.5 (9.8 ± 4.7, n = 34, Fig. 4f) with an overall scattered decreasing trend along the salinity gradient except one high point at salinity 27.6. Chlorophyll-a concentration did not show clear trend along the salinity gradient, but varied seasonally (Fig. 4g), typically being 3 times lower in the wet season (1.50 ± 0.52 μg L^{-1}, n = 10) than in the dry seasons of 2014 and 2015 (4.4 ± 1.3 μg L^{-1}, n = 26). Pheophytin was always lower than Chl-a and ~ 2
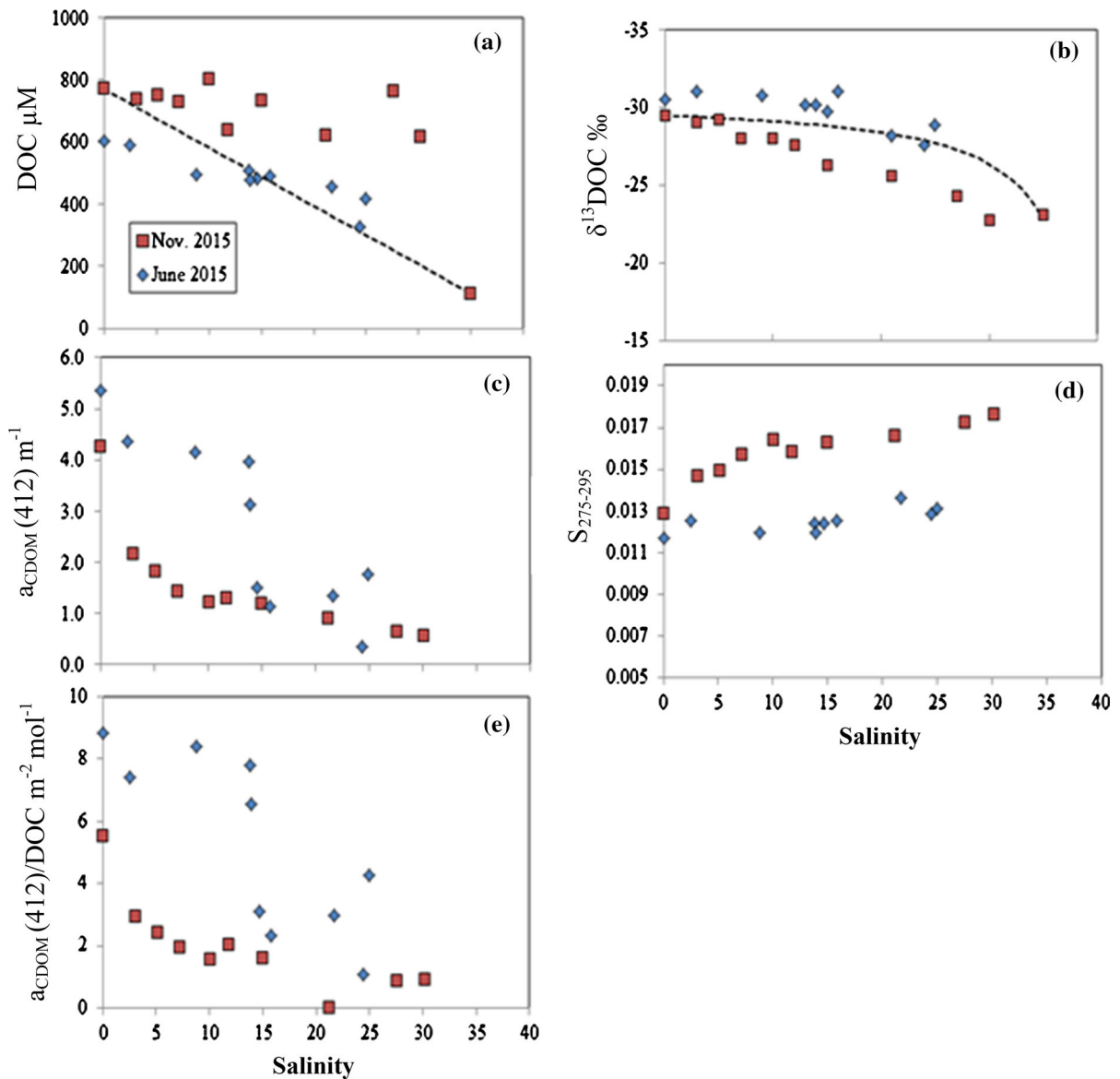
Fig. 3 **a** Distribution of DOC (μM) as a function of salinity and season (red squares as Nov 2015; blue diamonds as June 2015) **b** DOC $\delta^{13}C$ (‰), and **c, d, e** CDOM parameters absorption at 412 nm, slope at 275–295 nm and CDOM normalized to DOC in surface water along the salinity gradient. The predicted two fold greater end-member conservative mixing distributions of DOC versus salinity and of $\delta^{13}C$-DOC are shown as black dotted curves in a and b, assuming the observed end-members: marine DOC = 112 μM, DOC $\delta^{13}C$ = − 22.8‰; and river DOC = 770 μM, $\delta^{13}C$ = − 29.5‰

fold greater Chl-a/Pheo ratios were observed in the dry seasons (3.1 and 4.0 in October 2014 and November 2015, respectively) compared to the wet season (1.5, in June 2015) (see Table S2). The POC/Chl-a ratio (contribution of live biomass to the POC pool) was highest in the riverine zone in May 2015; on a seasonal basis this ratio was consistently higher in the wet than in the dry seasons (468 ± 164 versus 158 ± 120; Fig. 4h).

The percentages of TOC and TN with their isotopes and atomic ratios in the sediment, *Avicennia* leaves, litter and mixed microphytobenthos (MPB) slightly varied with mangrove age (Table 3). Mean value of TOC and $\delta^{13}C$ of sediment, leaves, litter and mixed MPB were 1.05 ± 0.4% and − 25.8 ± 0.07‰,

Table 3 The C, N elemental and stable isotopes (δ^{13}C ‰, δ^{15}N ‰), [TOC:TN] atomic ratios, of sediments (upper $\sim$ 2 cm), *Avicennia* leaves, litter, mixed microphytobenthos (MPB) and suspended matter, and pore water DOC (in µM, upper $\sim$ 2 cm) during both seasons in the four stages of mangrove development (BS: bare sediment; PM: pioneer mangrove; YM: young mangrove; AM: adult mangrove)

	TOC %	TN %	δ^{13}C ‰	δ^{15}N ‰	[TOC:TN]
Surface sediment					
BS	0.92	0.10	− 25.8	4.3	10.7
PM	0.85	0.12	− 24.2	4.6	8.3
YM	0.82	0.15	− 25.8	4.4	6.4
AM	1.63	0.20	− 27.6	3.8	9.5
Mean ± SD	1.05 ± 0.4	0.14 ± 0.04	− 25.8 ± 0.07	4.3 ± 0.3	8.7 ± 1.8
Avicennia leaves					
PM	44.1	3.38	− 28.4	1.5	15.2
YM	41.6	3.28	− 29.5	4.3	14.3
AM	39.7	3.43	− 33.6	3.1	13.5
Mean ± SD	41.8 ± 2.2	3.36 ± 0.1	− 30.5 ± 2.7	2.9 ± 1.4	14.5 ± 0.8
Litter					
YM	39.1	1.73	− 29.5	2.9	26.4
AM	37.5	1.65	− 30.7	2.2	26.5
Mean ± SD	38.3 ± 1.1	1.69 ± 0.05	− 30.1 ± 0.8	2.6 ± 0.05	26.4 ± 0
Mixed MPB					
PM	1.05	0.16	− 20.7	4.7	7.6
YM	0.86	0.13	− 20.9	5.1	7.7
AM	1.74	0.20	− 21.1	4.5	10.1
Mean ± SD	1.21 ± 0.5	0.16 ± 0.03	− 20.9 ± 0.2	4.6 ± 0.3	8.82 ± 1.4
Suspended matter					
Wet season	1.60	0.18	− 38.9	1.7	9.52
Dry season	1.48	0.18	− 37.7	0.8	12.81
Mean ± SD	1.54 ± 0.1	0.18 ± 0	− 38.3 ± 1.0	1.3 ± 0.6	11.16 ± 2
Pore water	DOC (µM)				
BS	1709				
PM	1847				
YM	1151				
AM	964				
Mean ± SD	1418 ± 426				

SD Standard deviation

41.8 ± 2.2% and − 30.5 ± 2.7‰, 38.3 ± 1.1% and − 30.1 ± 0.8‰, and 1.21 ± 0.5% and − 20.9 ± 0.2‰, respectively. Sediment and mixed MPB showed δ^{15}N enrichment (mean 4.3 ± 0.3‰ and 4.6 ± 0.3‰, respectively) compared to leaves and litter (2.9 ± 1.4‰ and 2.6 ± 0.05‰, respectively). The TOC % and [TOC:TN] atomic ratio of surface sediment and mixed MPB were lowest in the young mangroves (0.82% and 6.4 respectively) compared to other mangrove stages (0.85–1.63% and 8.3–10.7, respectively).

Dissolved Inorganic Carbon

During each sampling period (2013–2015), pH level increased along the salinity gradient with low inter-annual variability (Fig. 5a), and water was acidic at salinity 0 (pH 6.13 ± 0.34, stations: G11, R2, Riv1, OW1014, OW713) and basic at salinity 35 (pH 7.83, station G1). Similar to pH, total alkalinity (TA) of surface waters varied over a wide range (from 0.01 to 2.31 meq L^{-1}, n = 38), always with an increasing trend along the salinity gradient. The overall trend of TA mirrored the changes in DIC, which ranged between 0.04 and 2.19 mmol kg^{-1}S$_w$ (n = 46). Both TA and DIC showed nearly conservative mixing
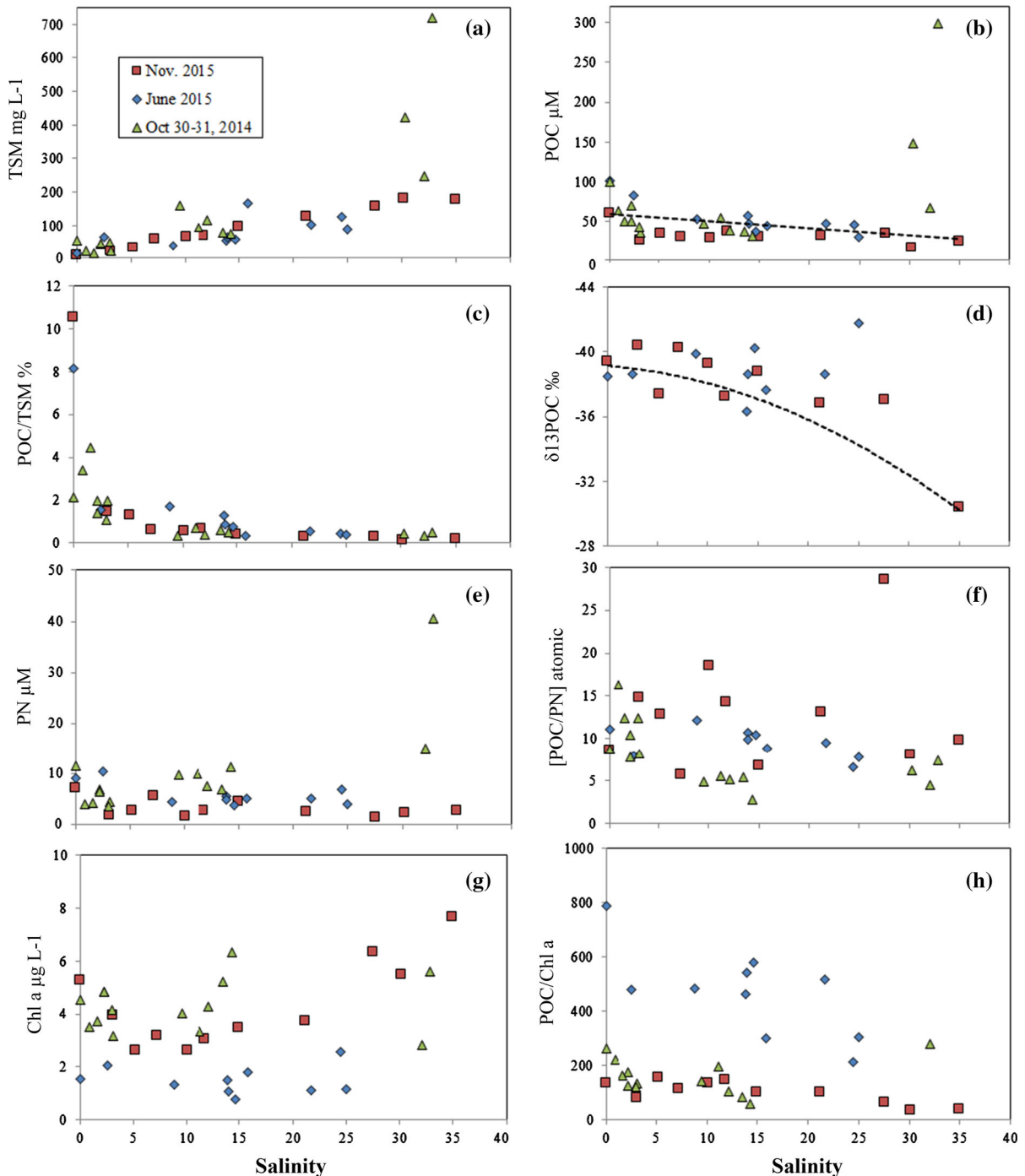
Fig. 4 Relative distribution of particulate organic matter (POC and PN, μM), δ^{13}C-POC (‰), total suspended matter (TSM in mg L^{−1}), Chl-a (μg L^{−1}) and different relative percentage

contributions highlighting the sources of POC in surface water along the salinity gradient in October (green triangles) 2014, June (blue diamonds) and November (red squares) 2015

patterns over the salinity range with minor seasonal and inter-annual variations (Fig. 5b, c). The pCO_2 values ranged between 599 and 5575 μatm (n = 21)

with similar trends between seasons (Fig. 5d). Lowest pCO_2 was recorded at M1 (599 μatm, S = 24.4) and highest at G10 (5575 μatm, S = 3.1). Along the

estuarine gradient, pCO_2 was particularly elevated but highly variable in the salinity range $\sim$ 2–15 irrespective of season (2650 $\pm$ 1470 μatm), whereas values were more stable at higher salinities (> 15) with relatively small variations in concentrations (860 $\pm$ 140 μatm). The $\delta^{13}DIC$ varied between $-20.7‰$ and $-5.0‰$ (n = 21) and increased

gradually with salinity in the dry season, while there was no clear trend in the wet season (Fig. 5e).

OC sources comparisons

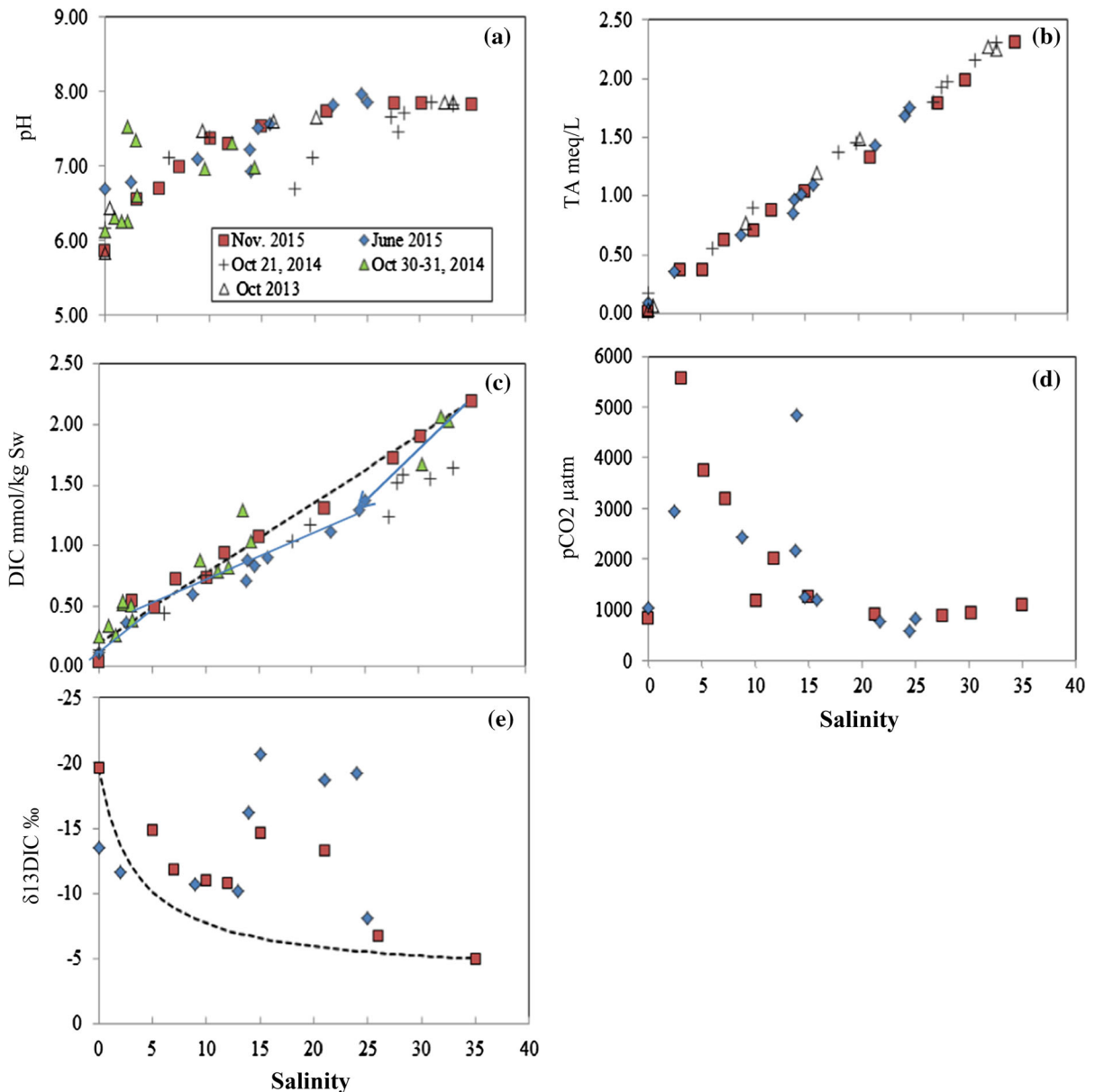Mean $\delta^{13}C$ of different measured OC sources (leaf, litter, marine/freshwater phytoplankton, MPB and

Fig. 5 a, b, c, d Relative distribution of pH, Total Alkalinity (meq/L), DIC (mmol kg^{-1}Sw), pCO$_2$ (μatm), and e δ^{13}C-DIC (‰) in surface water along the salinity gradient in October 2013 (blank triangles), October 2014 (green triangles and +), June (blue diamonds) and November (red squares) 2015. The

predicted two endmember conservative mixing distributions of DIC versus salinity and of δ^{13}C-DIC are shown as black dotted curves in d and e, assuming the observed endmembers: marine DIC = 2.2 mM, DIC δ^{13}C = $-5‰$; river DIC = 0.2 mM, DIC δ^{13}C = $-19.5‰$

surface sediment) are shown in Fig. 6. Freshwater phytoplankton was most depleted in ^{13}C ($- 36 \pm 4$‰, assumed after the observed values from the Orinoco River, Latin America by Hamilton and Lewis Jr. 1992) followed by *Avicennia* leaves and litter ($- 30.5 \pm 2.7$‰ and $- 30.1 \pm 0.8$‰, respectively), sediment ($- 25.8 \pm 1.4$‰), marine phytoplankton ($- 22 \pm 1.1$‰, assumed after Cifuentes et al. 1996), and mixed MPB ($- 20.9 \pm 0.3$‰). In the same plot observed mean δ^{13}C of DOC, POC and DIC across the entire salinity range in both seasons are given. The δ^{13}DOC values in the wet season ($- 29.8 \pm 1.2$‰) fell well within the uncertainty ranges of δ^{13}C of *Avicennia* leaves, litter and sediments and marine phytoplankton also added to the mixture in the dry season ($- 26.7 \pm 2.4$‰). The δ^{13}POC values in both dry and wet seasons were more negative than any of the measured endmembers falling outside their uncertainty ranges with the exception of the assumed freshwater phytoplankton value. The δ^{13}DIC appeared in the relatively heavier side of the x axis of Fig. 6, and laid between open ocean surface seawater ($\sim - 1.3$‰) and marine phytoplankton.

Estimates of nonconservative carbon inputs

The different endmember values of carbon forms observed during the dry season are: at $S_R = 0$, DOC = 770 μM, POC = 59.7 μM, DIC = 0.04 mol kg^{-1}, with δ^{13}C = $- 29.5$‰, $- 39.4$‰, and $- 19.6$‰, respectively; and at $S_M = 35$, DOC = 112 μM, POC = 25 μM, DIC = 2.19 mol kg^{-1}, with δ^{13}C = $- 23.1$, $- 30.4$, and $- 5$‰, respectively. Measured concentrations within the salinity gradient are clearly higher than predicted values for DOC with isotopic values being lighter than conservative predictions during the wet season and heavier during the dry season. In the case of DIC, the heaviest values within the estuary were during the dry season. Mean δ^{13}C$_{\Delta C}$ of the residual isotopic components for DOC, POC and DIC are $- 20.7 \pm 4$, $- 34.2 \pm 6$ and $- 38.5 \pm 18$‰, respectively. There is a large uncertainty in these estimates because they depend on estimating a relatively small difference between two large numbers (ΔC from Eq. 2). These results for the dry season are summarized in Table 4.

Discussion

The Sinnamary River interacts with a complex estuarine zone extending 10's of kms seaward from the coast. This region is characterized by inshore mangrove forests of various ages, tidal flats covered by extensive mats of microphytobenthos, bioturbated muds, and offshore mobile muds (Anthony et al.
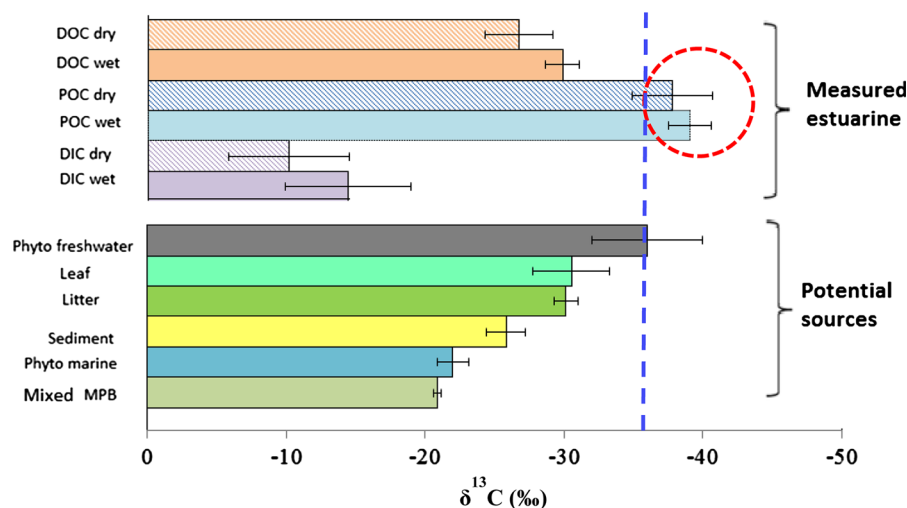

Fig. 6 Plot showing variations of δ^{13}C in different endmembers for identification of carbon sources in June (wet) and November (dry) 2015. The δ^{13}C of DOC, POC and DIC are mean values for the entire salinity range in each season. The δ^{13}C data for marine phytoplankton ($- 22 \pm 1.1$‰) and freshwater phytoplankton ($- 35 \pm 7$‰) were assumed from Cifuentes et al. (1996) and Hamilton and Lewis Jr. (1992), respectively. Red dotted circle marks a big isotopic deviation of POC from δ^{13}C of potential endmembers (except freshwater phytoplankton)

2010; Aschenbroich et al. 2016, 2017). Intertidal areas are dissected by networks of channels that are filled and emptied as mangroves are flooded or drained (see the satellite map in Fig. 2). Water having a wide range of salinity, e.g., 0–25, interacts and exchanges with mangroves, particularly those in the younger growth stages < 1–5 years old along the forest edges (Fig. 2). Thus, a spectrum of potential sources or sinks of POC, DOC, and DIC is present that can dynamically influence water column distributions and determine the net export or import of OC from or into the estuarine zone. It is not possible given this spatial and temporal complexity to accurately constrain OC fluxes through the Sinnamary estuary; however, we can identify primary controlling processes, the source and nature of material exported or imported, and infer the likely magnitude of fluxes. To do so, we utilize endmember mixing models along the salinity gradient (river, marine), as conceptual references and the deviation of concentration and isotopic measurements from model distributions as a basis for inferring processes and the relative importance of sources or sinks of OC.

Spatio-temporal dynamics of dissolved organic carbon (DOC)

DOC was the major form of organic carbon in the Sinnamary estuarine zones with DOC:POC ratios ranging between 4.5 and 37. Measured DOC concentrations in the Sinnamary River mouth sites are generally higher (604–770 μM, n = 2) than previous records available for the area from Gadel et al. (1997) (293–407 μM, n = 3) but comparable with the upper limit of Abril et al. (2005) (213–595 μM, n = 42). These Sinnamary river mouth sites are impacted by the mangrove drainage, thus mangrove-derived DOC can increase the pool whereas Abril et al. (2005) sampled over a considerable section of river not all of which is

impacted by mangrove drainage (e.g. mid and upper stretches). Globally, DOC concentrations of FG mangrove drainage and estuarine waters are similar in range but slightly lower than the Floridan everglades (141–1492 μM, S = 6.4–29.8; Romigh et al. 2006) and New Caledonia mangroves (693–954 μM, S ~ 4.5–33; Leopold et al. 2016). FG DOC concentrations are also higher than the values reported for mangroves from North Brazil (mean 360 μM, S = 0–35; Dittmar et al. 2001), South-East Brazil (191–290 μM, S = 24–32; de Rezende et al. 2007), Indian Sundarbans (214–328 μM, S = 31–26; Ray et al. 2015), Africa (80–220 μM, S = 35–38; Bouillon et al. 2007), Australia (80–200 μM, no freshwater input; Maher et al. 2013) and Middle East Persian Gulf (300–380 μM, S ~ 38–39, Ray et al. 2016). Given that the FG system has one of the highest reported mangrove height growth rates (150 cm yr^{-1}, Proisy et al. 2009), high DOC concentration could be also due to enhanced production of OC per tree that ultimately enriches the DOC concentration in the adjacent estuary due to the contribution of plant-derived humic substances leaching from forest sediment and enhanced litter fall (Richard et al. 2000).

If a seasonally invariant marine DOC concentration is assumed to be ~ 100 μM at S = 35, DOC distributions within the water column clearly showed deviation from simple conservative mixing models between river and marine endmembers during both the wet and dry seasons (shown as lines in Fig. 3a). It is clear that DOC is contributed to the water column from sources associated with a range of salinities from 0 to ~ 25, not only the Sinnamary River, consistent with net inputs from mangrove and tidal flat sources throughout the estuary (e.g., Figs. 1, 2). The differences in DOC concentrations between the wet (lower DOC) and dry (higher DOC) seasons could be primarily due to a dilution effect by an increased flux of water with low DOC and a generally lower

Table 4 Measured and expected values of concentration (μM for DOC and POC, mmole kg^{-1} for DIC), isotope estimates (‰), nonconservative residual concentration (ΔC) and isotopic component (δ^{13}C$_{ΔC}$) of DOC, POC and DIC

C$_{component}$	C$_{obs}$	C$_{mix}$	^{13}C$_{obs}$	^{13}C$_{mix}$	ΔC	δ^{13}C$_{ΔC}$
DOC	661 ± 192	441 ± 198	− 26.7 ± 2.4	− 28.1 ± 1.6	221 ± 194	− 20.7 ± 4
POC	31.8 ± 12	44.8 ± 9	− 37.5 ± 3.0	− 35.8 ± 2	− 13.1 ± 3	− 34.2 ± 6
DIC	1.11 ± 0.7	1.12 ± 0.6	− 11.5 ± 4.4	− 6.1 ± 2.6	− 0.01 ± 0.1	− 38.5 ± 18

Data are from the dry season only

residence time of water within the estuary relative to DOC production from mangroves during the wet season, resulting in a factor of 1.3 decrease in DOC compared to the dry season.

Previous studies have shown that mangrove-derived litter leaching and pore water seepage are the dominant pathways of terrigenous DOC and CDOM inputs from estuarine mangroves to the coastal ocean (Scully et al. 2004; Dittmar et al. 2006; Bouillon et al. 2007a; Shank et al. 2010; Bergamaschi et al. 2012; Cawley et al. 2013). In French Guiana, 3 to 4-fold higher DOC in pore water than in tidal water provides a reasonable source for export of litter-sourced DOC via tidal pumping and pore water seepage during the ebb (Table 3). The latter mechanism would be amplified by the bioturbation activities within this area (Aschenbroich et al. 2016, 2017). Similar conclusions were drawn for other mangrove environments (e.g. Tana estuary in Kenya, Bouillon et al. 2007b; tidal creek in Tanzania, Bouillon et al. 2007a; mangrove creek in Australia, Maher et al. 2013). It is noteworthy that some of the highest litter fall rates were recorded previously for FG mangroves (mean 6.4 t C ha^{-1} yr^{-1}; 25-months study by Betoulle et al. 2001) compared to the similar old forests like the Sundarbans (mean 4.6 t C ha^{-1} yr^{-1}; 30-months study by Ray et al. 2011), the world's largest mangrove forest. However, the Amazonian rainforest exhibited higher values (mean 8.7 t C ha^{-1} yr^{-1}, 12-months study by Nascimento et al. 2006). Litter loads should enrich the estuarine DOC pool via leaching (Dittmar et al. 2001); this process might be persistent throughout the rainfall period whereas during the dry season, it would be replaced by marine phytoplankton inputs at higher salinity (range 28–35).

Isotopic indicators of sources and fate of DOC

In addition to the distribution of DOC concentrations and deviations from a simple river–marine mixing model, C isotopic compositions are consistent with inputs of DOC across a range of salinities. There is a clear overall gradient from relatively negative δ^{13}C-DOC (– 29.5‰ to – 32‰) reflecting riverine and mangrove drainage sources to a heavier marine dominated composition (– 23‰; Fig. 3b). The DOC isotopic distributions deviate from a two endmember conservative mixing model during both seasons (dashed curve in Fig. 3b). During the dry season,

nonconservative DOC components estimated by subtracting the values of DOC predicted from the two endmember mixing model from the actual observed values of DOC (Eq. 2) revealed addition of 221 ± 194 μM DOC with δ^{13}C$_{ΔC}$ of – 20.7 ± 4‰ into the estuary (as +ΔC, Table 4), implying heavy δ^{13}DOC inputs sourced from marine phytoplankton or MPB or a mixture of both. In the wet season, although DOC concentrations are generally lower than in the dry season, there was a greater dominance of isotopically light terrigenous DOC inputs into the estuary as shown by the δ^{13}C depletion pattern (– 27.5 to – 31‰) (Fig. 3b). These isotopic data imply that mangroves are the primary contributor to DOC at low salinities because mangroves are C3 plants with δ^{13}C values ranging from – 29.4 to – 27‰ whereas C4 plants (e.g. sea grass, salt marsh), marine algae (phytoplankton) or benthic algae (e.g. MPB on FG tidal flat) have higher δ^{13}C values (– 10 to – 18.5‰, – 20 to – 22‰ and – 16.1‰, respectively; Bouillon et al. 2008; Gontharet et al. 2014). It appears that the initial mangrove-derived DOC is either sustained as the primary source in the estuary at the relatively short water residence times characterizing the high flow wet season, or is significantly modified by addition of heavier DOC derived from marine sources during dry periods with longer residence times of water within the estuary.

Sources and fate of CDOM

The general trend, ranges and mean values of a$_{cdom}$(412) observed in this study agree overall with those found in FG by Vantrepotte et al. (2015). The latter ascribed it to the high terrestrial influence on DOM pool. We further suggest that litter-leached high molecular weight DOM driven by monsoonal surface run-off in the estuary results in high CDOM absorption in the wet season compared to the dry season, consistent with the isotopic patterns discussed previously. This hypothesis is supported by lower S$_{275–295}$ in the wet season, emphasizing mangrove terrestrial input (i.e. litter leaching) to the DOM pool, while in the dry season, marine phytoplanktonic OC (characterized by higher S$_{275–295}$) would replace the terrestrial source as a result of more mixing of marine water during the flood. Helms et al. (2008) established S$_{275–295}$ as a potential optical descriptor for assigning terrestrial origin in CDOM. Spencer et al. (2012)

suggested that increasing values in $S_{275-295}$ are related to the decrease in molecular weight and aromaticity of CDOM from fresh to marine waters. We further found a good correlation between $S_{275-295}$ and $\delta^{13}DOC$ (linear regression equation: $\delta^{13}DOC = 971.S_{275-295} - 42.3$, $r^2 = 0.72$, $p < 001$, $n = 20$) which could serve as potential proxies for identifying DOM sources in mangroves waters. In this study, the colored content in the DOM pool was 2.6 times higher in the wet season ($a*_{cdom}412_{wet} > a*_{cdom}412_{dry}$): the detrital sources would release humic-type yellow substances losing aromaticity (per the colored content) after mixing and dilution with sea water further offshore.

The dry season shows a dilution gradient of terrigenous DOM concentrations and optical properties with increasing salinity, which is also reflected in increasing $\delta^{13}DOC$ along the gradient. In the wet season, on the other hand, in addition to lower salinity due to rainfall and the increase in river flow, the riverine and marine water masses did not completely mix in surface waters. There was a very marked halocline observed visually and from salinity measurements around salinity 15 on June 8th, 2015. Up to this salinity, the mangrove DOM signal dominated in surface water together with the strong vertical stratification of the water column: the intrusion of marine water in the inner part of the estuary during the rising tide occurred at depth as shown by the YSI probes deployments the following day (data not shown; salinity variations were recorded from 15 to 300 cm water depth). For higher salinities (> 15) in the outer part of the estuary, the river-mangrove signal was replaced by the marine signal in surface water. Optically the concept of distributed DOM sources from mangroves between salinities 0–15 appear consistent with the concentration and isotopic DOC data. The abrupt variations of $a*_{cdom}(412)$ in surface waters illustrate the tracing of these two water masses of different composition in colored DOM during the wet season. Between 0 and 15 of salinity, the values of $a*_{cdom}(412)$ are between 6 and 8.5 in $m^2\ mol^{-1}$ whereas these values are much lower for offshore waters ($< 2\ m^2\ mol^{-1}$). The latter changes in $a*_{cdom}(412)$ along the salinity gradient during the wet season tend to confirm the presence of two distinct water masses showing different DOM properties. Specifically, estuarine waters ($S < 15$) are characterized by highly chromophoric DOM when compared to the marine waters ($S > 15$). Such apparent non-conservative pattern for CDOM, which is not translated by a similar pattern in DOC, will be investigated more specifically in the future with a true 'marine reference' in the wet season which is missing in the current study.

Spatio-temporal dynamics of particulate organic matter (POM)

Sources and fate of suspended POM

In 2015, an almost two-fold higher POC content in TSM in the wet season relative to the dry season could be attributed to the monsoonal run-off and rapid flushing of mangrove-derived organic carbon that might be either litter debris or benthic microalgae resuspended on the tidal flat. 70% of the POC:PN ratios fell within the range 8 to 28 (Fig. 4f), indicating that POM was sourced from both terrigenous and benthic algae regardless of the seasons. Furthermore, consistent decline of POC/Chl-a ratios up to salinity 15, particularly in the dry seasons of 2014–15, suggests a continuous supply of benthic algae (i.e. MPB) to the POC pool, while lower values in the marine zone would result from higher contribution of marine phytoplankton. Two recent studies by Aschenbroich et al. (2016, 2017) showed the enrichment of pioneer mangroves tidal flats in Chl-a content (12 to 14 $\mu g\ g^{-1}$ sed.) compared to other facies (2 to 5 $\mu g\ g^{-1}$sed. in bare sediments and young mangroves) emphasizing the contribution of live MPB (Chl-a/Pheo in TSM was always > 1) to the organic carbon pool. Our additional measurements of benthic chloropigments (0–6 cm depth, in wet and dry seasons of 2015) resulted in the same trend of much higher Chl-a content and biomass at the pioneer sites (7–46 $\mu g\ g^{-1}$ sed. and 85–420 $mg\ m^{-2}$, respectively) compared to the other mangrove facies (1–4.5 $\mu g\ g^{-1}$sed. and 2–18 $mg\ m^{-2}$, respectively) further highlighting the resuspension of MPB from the vegetated tidal flat (i.e. mainly from pioneering facies) to the coastal water.

From Eq. 4, the highly negative $\delta^{13}C_{\Delta C}$ value ($- 34.2 \pm 6‰$) of the POC pool suggests the net input of an isotopically light C component that could reflect freshwater phytoplankton being an important source along the entire salinity gradient, at least in the dry season. The riverine $\delta^{13}DIC$ values between $- 20$ and $- 12‰$) might be the result of the degradation of the lighter POC from freshwater phytoplankton. On

the other hand, during wet season, high discharge and surface run off introduced more mangrove-derived POC (as eroded sediment and litter debris) as the primary source at the relatively short water residence times. This inference is also supported by relatively lower Chl-a/Pheo ratios in the wet season, highlighting the lack of fresh OM in the POC pool. POC and PN were strongly correlated during both seasons ($R^2 = 0.86$) indicating the same origin (i.e. MPB plus freshwater phytoplankton) of the particulate organic matter (Fig. 7).

In the lowest salinity riverine zone, however, a possible explanation for consistently negative isotopic values of POC, other than seasonal signal by freshwater phytoplankton, could be the presence of methane (CH_4)–derived POC inputs from the Petit-Saut reservoir (hydroelectric dam), located at Sinnamary upstream and emitting significant methane and carbon dioxide (Abril et al. 2005; Guérin et al. 2006). De Junet et al. (2009) reported similar depleted $\delta^{13}POC$ values ($-33.2‰$, $-31.6‰$) for the Sinnamary upper and middle stretch, ascribing it to the methanotrophic source and enhanced CH_4 oxidation in the water column. The commissioning of the dam in 1994, later led to deoxygenation of the water in the Sinnamary downstream, promoting CH_4 emission (Dumestre et al. 1997; Richard et al. 2005). In the Amazon estuary, Abril et al. (2013) reported also evidence of methane oxidation leading to a $\delta^{13}DIC$ pool up to $-55‰$. We hypothesize that CO_2 already depleted in ^{13}C from CH_4 oxidation could contribute to the photosynthetic C pool along with other sources.

In the estuarine region, relatively negative isotopic compositions of POC could also reflect the presence of methane (CH_4)–derived POC in the water column coming with eroded sediment of the senescent mangroves (old stands) that border the region (Fig. 2). Stable isotope values of CH_4 emitted from the wetlands may vary over a wide scale of -55 to $-70‰$ ($-59.6‰$ to $-65.2‰$ in a subtropical mangrove estuary in Australia reported by Maher et al. 2015). In this study, remote sensing data (Table 2; Fig. 2) showed that mature stands (30–50 years) constitute a major fraction of the mangrove area ($\sim 41\%$ relative to the total mangroves). These mature stands are composed of mixed and senescent trees and are situated at the left bank of the estuary where numerous small and big channels can be found (Fig. 2). These mangroves are still inundated part of
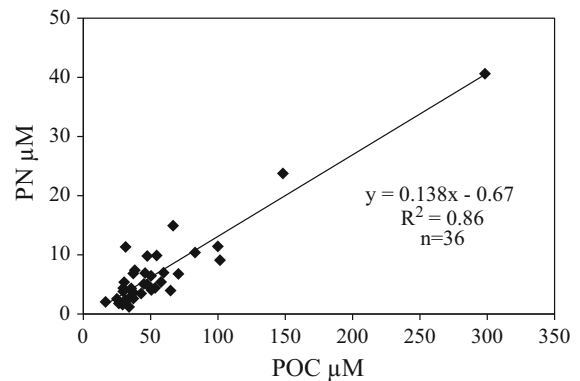

Fig. 7 Correlation between organic carbon and nitrogen in total suspended matter collected in surface water in October 2014, June and November 2015 (data of the three sampling times included)

the year (at spring tide) and anoxic sediment would allow reduced gas formation (dominantly methane and hydrogen sulphide). Although CH_4 measurements were not done in these areas, emission from bottom sediment and delivery of methanogenic POC through channels (mainly from eroded sediment of mature mangroves) seems likely.

Sources of sedimentary TOC, TN

Due to spatial heterogeneity and combinations of biotic (bioturbation activities by benthic fauna and root structure; Aschenbroich et al. 2016, 2017) and abiotic factors (sediment T, pH, redox potential; Marchand et al. 2003), the percentages of TOC and TN vary between facies and with depth in the normally suboxic–anoxic sediments of FG mangroves. Detailed discussion about these bio-physical factors is beyond the scope of the present study, but several general patterns can be noted. The sedimentary C pool, at least initially and at depth in deposits, is controlled by marine imports (off shore mobile mud) and mangrove effects are superimposed (marine POC import; terrestrial DOC export; CO_2 efflux). It is assumed that intense mineralization in mangrove stabilized mudbanks is initially sustained by labile OC transported shoreward from reactive mobile muds migrating along the coast ($\leq 0.7\%$ OC; Aller and Blair 2006). Furthermore, OC % ($1.21 \pm 0.5\%$) for the MPB samples indicates that these samples are a mixture of MPB and mineral material (and hence, also bulk organic matter from the sediment), rather than being

'pure' microphytobenthos for which we would expect OC of 40–50%. The $\delta^{13}C$ of mixed MPB in Sinnamary, $-20.9‰$, was more negative than similar samples from Makouria mudbank to the east ($-16.1‰$, Gontharet et al. 2014). Using the isotopic mixing model outlined previously (Eqs. 1–4), and assuming end-member contributions from bulk sediment with OC = 0.5–0.7% and mean $\delta^{13}C = -24.72‰$ (Aller and Blair 2006), then the estimated MPB contribution to the sample mixture varied from 0.51 to 0.71% OC with a range of MPB-estimated isotopic values of -15.7 to $-18.2‰$ (mean = $-17‰$).

Two endmember analysis (mixed MPB, mangrove) suggests that mixed MPB mainly contributed to surficial OC on the Sinnamary mudbank and tidal flat ($\sim 100\%$ for pioneer mangroves) while litter dominated in older stages ($\sim 80\%$ for young mangroves). Sedimentary organic carbon of the *Avicennia* mangrove forest is a blend of allochthonous and autochthonous constituents. Due to less inundation and tidal flushing in the adult mangrove forest, OC % was higher in the mature forest stage than in the other facies (Table 3). Overall, sediment OC % (0.9–1.63%, Table 3) was lower in this study, compared with Indo-Pacific mangroves (1.8–18%; Donato et al. 2011), but similar to the previous studies by Marchand et al. (2003) (0.7–2.0%), Gontharet et al. (2014) (0.8–1.0%) and Aschenbroich et al. (2016) (0.7–1.0%) in FG mangroves.

With respect to isotopic patterns in sediment associated with the stages of mangrove development along the coastal system, Showers and Angle (1986) and Aller and Blair (2006) reported an increase in the bulk $\delta^{13}C$ of OC from $-28‰$ at the Amazon River mouth, to $-25.6‰$ in deltaic topset deposits, and $-24.7‰$ in bare mudbanks along French Guiana (similar to this study, $-25.8‰$). This result suggests additional marine component(s) in the mobile mud of French Guiana and net loss of terrestrial OC during alongshore transit. Gontharet et al. (2014) found the sedimentary OM of Macouria mudbank in French Guiana ($\delta^{13}C$ ranging from $-24.9‰$ to $-23.4‰$) to be a mixture of *Avicennia* leaves and mixed MPB ($\delta^{13}C$: $-27.3‰$ and $-16.1‰$, respectively). Microbial and fungal activities are known to induce intense processing of OM in mangrove sediments, resulting in 15.3% enrichment of heavy carbon in sediment OM compared to plant leaves (Ehleringer et al. 2000).

Mixed MPB could account for the lower ranges of $\delta^{15}N$ recorded in the sediment (mean of 4.3‰ vs. 4.6‰ for MPB) relative to mangrove leaves (2.9‰). N$_2$-fixing cyanobacteria within the MPB are known to be the main source of bioavailable nitrogen in the mangroves (Voss et al. 2011). Another complementary study in 2015 (B. Becker, LEMAR, pers. comm.) also found the dominance of cyanobacterial assemblages in the Sinnamary mangrove area, particularly for the pioneer and young mangrove stages.

Spatio-temporal dynamics of dissolved inorganic carbon (DIC)

Distribution and sources of DIC

The distribution of water column DIC, which is the dominant C pool at S > 10, reflects a balance between river and marine endmember mixing and complex patterns of sources and sinks within the estuary. Both TA and DIC show apparent overall linear mixing patterns along the Sinnamary salinity gradient regardless of season. However, there are apparently sub-regions of subtle variations not explained by a single linear relationship between river and ocean endmembers (Fig. 4b, c), and DIC speciation and isotopic distributions demonstrate dynamic source–sink reaction processes, particularly within the salinity range 0–25. Additional DIC sources include water column and benthic remineralization of DOC and POC, and sedimentary carbonate dissolution. DIC sinks include photosynthesis and carbonate mineral precipitation, both of which can be especially intense in surface sediments during ebb tide due to growth of microphytobenthic mats and dessication (evaporite mineral precipitation).

Assuming that the small variations of water column DIC are real and not a combination of measurement uncertainty and mixing heterogeneity, there is an apparent zone of rapid net increase in DIC between 0–4 salinity, a zone from salinity 4–25 indicating a small net consumption, and then a regular increase to marine values (refer to wet season trend in Fig. 5c). The pH distributions and corresponding calculated pCO_2 patterns are consistent with dominant remineralization and net CO_2 production in the lowest salinity ranges (0–5), but net consumption within the salinity 5–25 (Fig. 5, a, d). Overall, pCO_2 was elevated, highly variable and dynamic at the lower salinities (10 fold

less than riverine value of Abril et al. 2005), a behavior confirmed by high resolution time series measurements (Ray et al. in prep.). Maher et al. (2015) support the idea that pCO_2 can be highly variable in water inundating and draining mangroves.

For salinities in the range 0–15, supersaturated pCO_2 ($\sim$ 800–6000 µatm) and progressive net uptake, low pH (5.86–7.54), O_2 under-saturation (66–86%) and consistent depletion of δ^{13}C-DIC (maximum up to − 20‰ at S = 15) were observed (Fig. 5), highlighting the complex interaction of both photosynthesis (CO_2 uptake) and respiration of OM (isotopically light DIC) within the estuarine zone. Remineralization of both DOC and POC favored by high water temperature in the estuary could drive pelagic respiration and explain the relatively high pCO_2. On the other hand, the enrichment of δ^{13}DIC (max. − 4.5‰) and lowering of pCO_2 for higher salinities (20–35) would first reflect the mixing of high-DIC seawater (2.2 mmol kg^{-1}) with low-DIC freshwater (< 0.1 mmol kg^{-1}) and second enhanced uptake of DIC by phytoplankton (Middelburg and Nieuwenhuize 1998). There is more evidence for net respiration of OM during the wet season (scattering of depleted δ^{13} DIC in the salinity range 0–25, Fig. 5e). Strong isotopic deviations between observed and expected δ^{13}DIC as well as negative Δ^{13}C (− 5.5 ± 1.8‰) indicate consistent addition of inorganic C to the mangrove estuary. The non-conservative DIC component ($\delta^{13}C_{\Delta C}$= − 38.5 ± 18‰) in the lower salinity region ressembles the isotopic signal of the POC pool, likely reflecting freshwater phytoplankton or CH_4 derived components as a source of remineralized carbon. In contrast, offshore pore water DIC is relatively heavy (− 19.2 ± 0.5‰), suggesting the dominance of benthic and/or pelagic algae (as MPB and phytoplankton, respectively), and their rapid remineralization, despite much higher concentrations of isotopically depleted POC ($\sim$ − 24.7‰) in the solid phase (Aller and Blair, 2006).

The role of carbonate mineral dissolution and precipitation on DIC concentrations and isotopic compositions is difficult to evaluate but is clearly important. For example, halite, carbonates and gypsum obviously precipitate as exposed tidal flat muds become desiccated in the strong tropical sun. Similarly, CO_2 degassing that can modify both estuarine DIC and δ^{13}DIC (Miyajima et al. 2009), may be operating within the Sinnamary in tandem with other processes like dissolution and precipitation. However, a separate study would be required to constrain these processes.

Conclusions

In this study, spatio-temporal variations of DOC, POC and DIC concentrations with their isotopes provide critical data for revealing the biogeochemical functioning of the mangrove coastal systems in French Guiana. The mangrove-influenced Sinnamary estuary is richer in DOC compared to other mangrove regions such as the Brazilian, Indian Sundarbans, and African coasts. Both on seasonal and spatial bases, major changes in the distribution and sources of carbon pools were observed. The same physical processes associated with water residence times can explain part of the seasonality in DOC and POC concentrations. There was evidence of a very isotopically depleted OC pool, likely reflecting an initial CH_4 source from senescent mangroves and the Petit Saut hydroelectric dam, and POC derived from freshwater phytoplankton. In the FG system, there are strong linkages between intertidal mangrove forests and the estuary in terms of carbon export, exchange, and transformation via multiple processes such as, litter-leaching, pore water drainage, sediment erosion and biofilm resuspension, remineralization and lateral CO_2 transport and methanotrophy. However; there are active exchanges, and the system does not behave as if carbon were simply transported out of the mangrove system. In fact, most of the sedimentary C that forms the basis for sediment formation in the mangrove forest is from marine sources imported from the offshore mobile mud stream and colonized by mangroves. Because of the complex spatial patterns of mangrove distributions, tidal channels, and mudflats, and equally complex patterns of freshwater, pore water, and seawater mixing and transport, exactly how much DOC, POC and DIC are exported from the mangroves to the ocean (i.e. carbon outwelling), imported from the sea as marine plankton-rich sediment, and what fraction is respired locally by benthic organisms remain to be quantitatively determined.

References

Abril G and others (2014) Amazon River carbon dioxide outgassing fuelled by wetlands. Nature 505:395–398. https://doi.org/10.1038/nature12797

Abril G, Guérin F, Richard S, Delmas R, Galy-Lacaux C, Gosse P, Tremblay A, Varfalvy L, Santos MA, Matvienko B (2005) Carbon dioxide and methane emissions and the carbon budget of a 10-year old tropical reservoir (Petit Saut, French Guiana). Global Biogeochem Cycles 19:GB4007. https://doi.org/10.1029/2005gb002457

Abril G, Deborde J, Savoye N, Mathieu F, Moreira-Turcq P, Artigas F, Meziane T, Takiyama RL, de Souza MS, Seyler P (2013) Export of ^{13}C-depleted dissolved inorganic carbon from a tidal forest bordering the Amazon estuary. Estuar Coast Shelf Sci 129:23–27

Aller RC, Blair NE (2006) Carbon remineralization in the Amazon-Guianas tropical mobile mudbelt: a sedimentary incinerator. Cont Shelf Res 26:2241–2259

Alongi DM (2014) Carbon Cycling and Storage in Mangrove Forests. Annu Rev Mar Sci 6:195–219

Anthony EJ, Gardel A, Gratiot N, Proisy C, Allison MA, Dolique F, Fromard F (2010) The Amazon-influenced muddy coast of South America: a review of mud-bank–shoreline interactions. Earth-Sci Rev 103:99–121

Aschenbroich A, Michaud E, Stieglitz T, Fromard F, Gardel A, Tavares M, Thouzeau G (2016) Brachyuran crab community structure and associated sediment reworking activities in pioneer and young mangroves of French Guiana, South America. Estuar Coast Shelf Sci 182:60–71

Aschenbroich A, Michaud E, Gilbert F, Fromard F, Alt A, GarrecV Le, Bihannic I, De Coninck A, Thouzeau G (2017) Bioturbation functional roles associated with mangrove development in French Guiana, South America. Hydrobiol 794:179–202

Bauer JE, Bianchi TS (2011) Dissolved Organic Carbon Cycling and Transformation. In: Wolanski E, McLusky DS (eds) Treatise on Estuarine and Coastal Science, 5:7-67. AcademicPress, Waltham

Bergamaschi BA, Krabbenhoft DP, Aiken GR, Patino E, Rumbold DG, Orem WH (2012) Tidally driven export of dissolved organic carbon, total mercury, and methyl mercury from a mangrove-dominated estuary. Environ Sci Technol 46:1371–1378

Betoulle JL, Fromard F, Fabre A, Puig H (2001) Caractérisation des chutes de litière et des apports au sol en nutriments dans une mangrove de Guyane française. Can J Bot 79:238–249

Borges AV, Djenidi S, Lacroix G, The´ateJ, Delille B, Frankignoulle M (2003) Atmospheric CO_2 flux from mangrove surrounding waters. Geophys Res Lett 30: 1558. https://doi.org/10.1029/2003gl017143

Bouillon S, and others (2008) Mangrove production and carbon sinks: a revision of global budget estimates. Global Biogeochem Cycles 22: GB2013, https://doi.org/10.1029/2007gb003052

Bouillon S, Middelburg JJ, Dehairs F, Borges AV, Abril G, Flindt MR, Ulomi S, Kristensen E (2007a) Importance of intertidal sediment processes and porewater exchange on the water column biogeochemistry in a pristine mangrove creek (RasDege, Tanzania). Biogeosci 4:311–322

Bouillon S, Dehairs F, Schiettecatte LS, Borges AV (2007b) Biogeochemistry of the Tana estuary and delta (northern Kenya). Limnol Oceanogr 52:46–59

Buckingham S, Tipping E, Hamilton-Taylor J (2008) Dissolved organic carbon in soil solutions: a comparison of collection methods. Soil Use Manag 24:29–36

Canuel EA, Hardison AK (2016) Sources, Ages, and Alteration of Organic Matter in Estuaries. Ann Rev Mar Sci 8:409–434

Carpenter, I.H., Bradford, W.L., Grant, V. Processes affecting the composition of estuarine waters, p. 188- 214 In L. E. Cronin red.], Estuarine research. V. 1. Academic. 1975

Cawley KM, Yamashita Y, Maie N, Jaffé R (2013) Using Optical Properties to Quantify Fringe Mangrove Inputs to the Dissolved Organic Matter (DOM) Pool in a Subtropical Estuary. Estuar and Coast 37:399–410

Chen M, Maie N, Parish K, Jaffé R (2013) Spatial and temporal variability of dissolved organic matter quantity and composition in an oilgotrophic subtropical coastal wetland. Biogeochem 115:167–183

Cifuentes LA, Coffin RB, Solorzano L, Cardenas W, Espinoza J, Twilley RR (1996) Isotopic and elemental variations of carbon and nitrogen in a mangrove estuary. Estuar Coast Shelf Sci 43:781–800

De Junet A, Abril G, Gue´rin F, Billy I, de Wit R (2009) A multi-tracers analysis of sources and transfers of particulate organic matter in a tropical reservoir (Petit Saut, French Guiana). River Res Appl 25: 253-271

De Merona Bernard (2005) Le fleuve, le barrage et les poisons, Le Sinnamary et le barrage de Petit Saut en Guyane francaise (1989-2002). IRD Editions, Paris 2005. 135 pp

De Rezende CE, Lacerda LD, Ovalle ARC, Silva LFF (2007) Dial organic carbon fluctuations in a mangrove tidal creek in Sepetiba bay, Southeast Brazil. Braz J Biol 67:673–680

Debenay JP, Jouanneau JM, Sylvestre F, Weber O, Guiral D (2007) Biological origin of rhythmites in muddy sediments of French Guiana. J Coast Res 236:1431–1442

Dickson AG, Millero FJ (1987) A comparison of the equilibrium constants for the dissociation of carbonic acid in seawater media. Deep Sea Res Part A 34:1733–1743

Dittmar T, Lara RJ, Kattner G (2001) River or mangrove? Tracing major organic matter sources in tropical Brazilian coastal waters. Mar Chem 73:253–271

Dittmar T, Hertkorn N, Kattner G, Lara, RJ (2006) Mangroves, a major source of dissolved organic carbon to the oceans. Global Biogeochem Cycles 20: GB1012. https://doi.org/10.1029/2005gb002570

Donato DC, Kauffman JB, Murdiyarso D, Kurnianto S, Stidham M, Kanninen M (2011) Mangroves among the most carbon-rich forests in the tropics. Nature Geosci 4:293–297

Dumestre JF, Labroue L, Galy-Lacaux Reynouard C, Richard S (1997) Biomasses et activités bactériennes dans la retenue et à l'aval du barrage de Petit-Saut (Guyane):influence sur les émissions de méthane et la consommation d'oxygène. Hydroécol Appl 9:139–167

Ehleringer JR, Buchmann N, Flanagan LB (2000) Carbon isotope ratios in belowground carbon cycle processes. EcolAppl 10:412–422

Fabre A, Fromard F, Trichon V (1998) Fractionation of phosphate in sediments of four representative mangrove stages (French Guiana). Hydrobiologia 392:13–19

Fichot CG, Benner R (2011) A novel method to estimate DOC concentrations from CDOM absorption coefficients in coastal waters. Geophys Res Lett 38(3):L03610. https://doi.org/10.1029/2010GL046152

Fromard F, Puig H, Mougin E, Marty G, Betoulle JL, Cadamuro L (1998) Structure, above-ground biomass and dynamics of mangrove ecosystems: new data from French Guiana. Oecologia 115:39–53

Fromard F, Vega C, Proisy C (2004) Half a century of dynamic coastal change affecting mangrove shorelines of French Guiana. A case study based on remote sensing data analyses and field surveys. Mar Geol 208:265–280

Fuentes JD, Barr JG (2015) Mangrove forests and carbon and water cycling. Agr Forest Meteorol 13:263–265

Gadel F, Serve L, Blazi JL (1997) Traceurs organiques dans les suspensions et dans la matie're organique dissoute du fleuve Sinnamary—Barrage de Petit-Saut (Guyane française): sources et conditions du milieu. Hydroecol Appl. 9:115–138

Gattuso JP, Frankignoulle M, Wollast R (1998) Carbon and carbonate metabolism in coastal aquatic ecosystems. Annu Rev Ecol Syst 29:405–434

Gensac E, Gardel A, Lesourd S, Brutier I (2015) Morphodynamic evolution of an intertidal mudflat under the influence of Amazon sediment supply–Kourou mud bank, French Guiana, South America. Estuar Coast Shelf Sci 158:53–62

Gillikin DP, Bouillon S (2007) Determination of δ 18O of water and δ 13C of dissolved inorganic carbon using a simple modification of an elemental analyzer – isotope ratio mass spectrometer (EA-IRMS): An evaluation. Rapid Commun Mass Spectrom 21:1475–1478

Gontharet S, Mathieu O, Lévêque J, Lesourd S, Caillaud J, Gardel A, Sarrazin M, Proisy C (2014) Distribution and sources of bulk organic matter (OM) on a tropical intertidal mud bank in French Guiana from elemental and isotopic proxies. Chem Geol 376:1–10

Guérin F, Abril G, Richard S, Burban B, Reynouard C, Seyler P, Delmas R (2006) Methane and carbon dioxide emissions from tropical reservoirs: significance of downstream rivers. Geophys Res Lett 33:L21407. https://doi.org/10.1029/2006GL027929

Hamilton SK, Lewis WM Jr (1992) Stable carbon and nitrogen isotopes in algae and detritus from the Orinoco River floodplain, Venezuela. Geochim Cosmochim Ac 56:4231–4246

Hansson I (1973) A new set of acidity constants for carbonic acid and boric acid in seawater. Deep Sea Res 20:461–478

Helms JR, Stubbins A, Ritchie JD, Minor EC, Kieber DJ, Mopper K (2008) Absorption spectral slopes and slope ratios as indicator of molecular weight, source, and photobleaching of chromophoric dissolved organic matter. Limnol Oceanogr 53:955–969

Hettmann E, Brand WA, Gleixner G (2007) Improved isotope ratio measurement performance in liquid chromatography/isotope ratio mass spectrometry by removing excess oxygen. Rapid Commun Mass Spectrom 21:4135–4144

Ho DT, Ferrón S, Engel VC, Larsen LG, Bar JG (2014) Air-water gas exchange and CO$_2$ flux in a mangrove-dominated estuary. Geophys Res Lett 41:108–113. https://doi.org/10.1002/2013GL058785

Hutchison J, Manica A, Swetnam R, Balmford A, Spalding M (2014) Predicting Global Patterns in Mangrove Forest Biomass. Conserv Lett 7:233–240

Kennedy H, Gacia E, Kennedy DP, Papadimitriou S, Duarte CM (2004) Organic carbon sources to SE Asian coastal sediments. Estuar Coast Shelf Sci 60:59–68

Kuramato T, Minagawa M (2001) Stable carbon and nitrogen isotopic characterization of organic matter in a mangrove ecosystem on the southwestern coast of Thailand. J Oceanogr 57:421–431

Lamb AL, Wilson GP, Leng MJ (2006) A review of coastal palaeoclimate and relative sea-level reconstructions using d^{13}C and C/N ratios in organic material. Earth Sci Rev 75:29–57

Lehmann MF, Bernasconi SM, Barbieri A, McKenzie JA (2002) Preservation of organic matter and alteration of its carbon and nitrogen isotope composition during simulated and in situ early sedimentary diagenesis. Geochim Cosmochim Ac 66:3573–3584

Leopold A, Marchand C, Deborde J, Allenbach M (2016) Water Biogeochemistry of a Mangrove-Dominated Estuary under a Semi-Arid Climate (New Caledonia). Estuar Coast 40:773–791

Lewis E, Wallace DWR (1998) Program developed for CO$_2$ system calculations. Anal. Cent., Oak Ridge Natl. Lab., Oak Ridge, Tenn, Carbon Dioxide Inf

Loder TC, Reichard RP (1981) The dynamics of conservative mixing in estuaries. Estuar 4:64–69

Maher DT, Santos IR, Golsby-Smith L, Gleeson J, Eyre BD (2013) Groundwater-derived dissolved inorganic and organic carbon exports from a mangrove tidal creek: the missing mangrove carbon sink? Limnol Oceanogr 58:475–488

Maher DT, Cowley K, Santos IR, Macklin P, Eyre BD (2015) Methane and carbon dioxide dynamics in a subtropical estuary over a diel cycle: insights from automated in situ

radioactive and stable isotope measurements. Mar Chem 168:69–79

Maia de Oliveira CJ, Clavier J (2000) Space-time variations of suspended material in the Sinnamary estuary, French Guiana. Influence of Petit Saut electric dam). Rev bras oceanogr 48:29–39

Marchand C (2017) Soil carbon stocks and burial rates along a mangrove forest chronosequence (French Guiana). Forest Ecol Manag 384:92–99

Marchand C, Lallier-Verge s E, Baltzer F (2003) The composition of sedimentary organic matter in relation to the dynamic features of a mangrove-fringed coast in French Guiana. Estuar Coast Shelf Sci 56: 119–130

Marchand C, Baltzer F, Lallier-Vergès E, Albéric P (2004) Interstitial water chemistry in mangrove sediments in relationship to species composition and developmental stage. (French Guiana). Mar Geol 208:361–381

McLeod E, Chmura GL, Bouillon S, Salm R, Björk M, Duarte CM, Lovelock CE, Schlesinger WH, Silliman BR (2011) A blueprint for blue carbon: toward an improved understanding of the role of vegetated coastal habitats in sequestering CO_2. Front Ecol Environ 9:552–560

Middelburg JJ, Nieuwenhuize J (1998) Carbon and nitrogen stable isotopes in suspended matter and sediments from the Schelde estuary. Mar Chem 60:217–225

Mitchell BG, Kahru M, Wieland J, Stramska M (2003) "Determination of spectral absorption coefficients of particles, dissolved material and phytoplankton for discrete water samples," in *Ocean Optics Protocols for Satellite Ocean Color Sensor Validation*, J. L. Mueller, G. D. Fargion and C. R. McClain, eds. (NASA Goddard Space Flight Center, 2003)

Miyajima T, Tsuboi Y, Tanaka Y, Koike I (2009) Export of inorganic carbon from two Southeast Asian mangrove forests to adjacent estuaries as estimated by the stable isotope composition of dissolved inorganic carbon. J Geophys Res 114:G01024. https://doi.org/10.1029/2008JG000861

Mook WG, Tan TC (1991) Stable carbon isotopes in rivers and estuaries. In: Degens ET, Kempe S, Richey JE (eds) Biogeochemistry of Major World Rivers. SCOPE, John Wiley and Sons Ltd, pp 245–264

Nascimento RESA, Mehlig U, Menezes MPM (2006) Produção de serapilheiraem um fragmento de bosque de terra firme e um manguezalvizinhosnapenínsula de Ajuruteua, Bragança, Pará. Bol. Mus. Para. Emílio Goeldi, Ciências Naturais, Belé. 2:71–76

Officer CB (1976) Physical Oceanography of Estuaries (and Associated Coastal Waters). Wiley-Inter science, New York, p 465

Osburn CL, St-Jean G (2007) The use of wet chemical oxidation with high-amplification isotope ratio mass spectrometry (WCO-IRMS) to measure stable isotope values of dissolved organic carbon in seawater. Limnol Oceanogr: Methods 5:296–308

Strickland JDH, Parsons, TR (1968) A practical handbook of seawater analysis. Fish. Res. Board Can. 167

Proisy C, Couteron P, Fromard F (2007) Predicting and mapping mangrove biomass from canopy grain analysis using Fourier-based textural ordination of IKONOS images. Remote Sens Environ 109:379–392

Proisy C, Gratiot N, Anthony E, Gardel A, Fromard F, Heuret P (2009) Mud bank colonization by opportunistic mangroves: a case study from French Guiana using lidar data. Continental Shelf Res 29:632–641

Ralison OH, Borges AV, Dehairs F, Middelburg JJ, Bouillon S (2008) Carbon biogeochemistry of the Betsiboka estuary (north-western Madagascar). Organic Geochem 39:1649–1658

Ray R, Shahraki M (2016) Multiple sources driving the organic matter dynamics in two contrasting tropical mangroves. Sci Total Environ 571:218–227

Ray R, Ganguly D, Chowdhury C, Dey M, Das S, Dutta MK, Mandal SK, Majumder N, De TK, Mukhopadhyay SK, Jana TK (2011) Carbon sequestration and annual increase of carbon stock in a mangrove forest. Atmos Environ 45:5016–5024

Ray R, Rixen T, Baum A, Malik A, Gleixner G, Jana TK (2015) Distribution, sources and biogeochemistry of organic matter in a mangrove dominated estuarine system (Indian Sundarbans) during the pre-monsoon. Estuar Coast Shelf Sci 167:404–413

Raymond PA, Bauer JE (2001) DOC cycling in a temperate estuary: a mass balance approach using natural ^{14}C and ^{13}C isotopes. Limnol Oceanogr 46:655–667

Richard S, Galy-Lacaux C, Arnoux A, Cerdan P, Delmas R, Dumestre J-F, Gosse P, Horeau V, Labroue D, Sissakian C (2000) Evolution of physico-chemical water quality and methane emissions in the tropical hydroelectric reservoir of Petit-Saut (French Guiana). VerhInt Ver Limnol 27:1454–1458

Richard S, Grégoire A, Gosse P (2005) Efficacité d'un seuil artificiel sur l'oxygénation de l'eau et l'élimination de CH_4 contenu dans l'eau évacuée par la barrage hydroélectrique de Petit Saut (Guyane française). Revue des sciences de l'eau.18: 127–141

Romigh MA, David SE, Rivera-Monroy VH, Twilley RR (2006) Flux of organic carbon in a riverine mangrove wetland in the Florida coastal Everglades. Hydrobiol 569:505–516

Sarazin G, Michard G, Prevot FMP (1999) A rapid and accurate spectroscopic method for alkalinity measurements in sea water samples. Wat Res 33:290–294

Scheibe A, Krantz L, Gleixner G (2012) Simultaneous determination of the quantity and isotopic signature of dissolved organic matter from soil water using high-performance liquid chromatography/isotope ratio mass spectrometry. Rapid Commun Mass Sp 26:173–180

Scully NM, Maie N, Dailey SK, Boyer JN, Jones RD, Jaffe R (2004) Early diagenesis of plant-derived dissolved organic matter along a wetland, mangrove, estuary ecotone. Limnol Oceanogr 49: 1667–1678

Shank GC, Lee R, Vähätalo AV, Zepp RG, Bartels E (2010) Production of chromophoric dissolved organic matter from mangrove leaf litter and floating Sargassum colonies. Mar Chem 119:172–181

Showers WJ, Angle DG (1986) Stable isotopic characterization of organic carbon accumulation on the Amazon continental shelf. Cont Shelf Res 6:227–244

Spencer RGM, Butler KD, Aiken GR (2012) Dissolved organic carbon and chromophoric dissolved organic matter properties of rivers in the USA. J Geophys Res 117:G03001. https://doi.org/10.1029/2011JG001928

Sylvestre F, Guiral D, Debenay JP (2004) Modern diatom distribution in mangrove swamps from the Kaw Estuary (French Guiana). Mar Geol 208:281–293

Twilley RR, Chen RH, Hargis T (1992) Carbon sinks in mangroves and their implications to carbon budget to tropical coastal ecosystems. Water Air Soil Pollut 64:265–288

Vantrepotte V, Danhiez FP, Loisel H, Ouillon S, Mériaux X, Cauvin A, Dessailly D (2015) CDOM-DOC relationship in contrasted coastal waters: implication for DOC retrieval from ocean color remote sensing observation. Opt Express 23:33–54

Voss M, Wannicke N, Deutsch B, Bronk D, Sipler R, Purvaja R, Ramesh R, Rixen T (2011) In: Eric, W., McLusky, D., Walthmann (Eds.), Internal Cycling of Nitrogen and Nitrogen Transformations. Treatise on Estuarine and Coastal Science. Academic Press, Amsterdam, pp. 231–259

Walcker R, Anthony EJ, Cassou C, Aller RC, Gardel A, Proisy C, Martinez J-M, Fromard F (2015) Fluctuations in the extent of mangroves driven by multi-decadal changes in North Atlantic waves. J Biogeogr 42:2209–2219